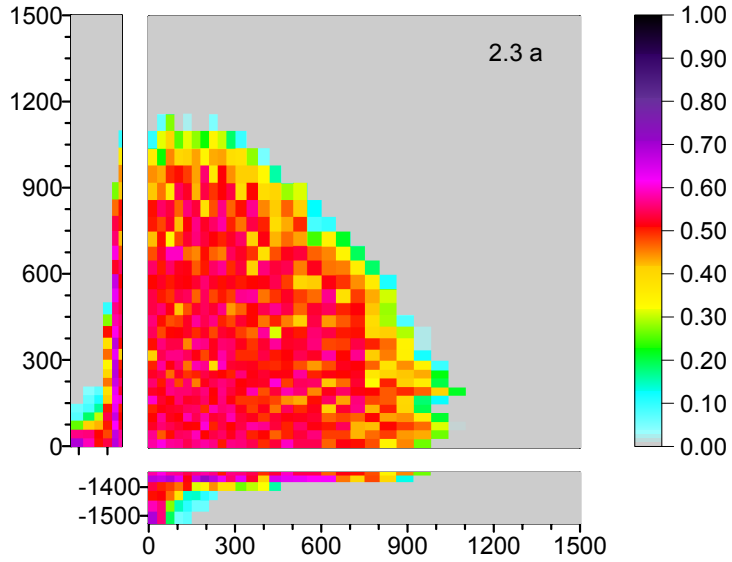

Hannover, Juli 2004

BGR Bundesanstalt für Geowissenschaften und Rohstoffe

CO_2 Storage Scenarios in North Germany

GESTCO Project Case Studies

Franz May, Paul Krull, Peter Gerling
Bundesanstalt für Geowissenschaften und Rohstoffe

Hannover, Juli 2004

Table of Contents:

Two scenarios have been composed for CO_2 storage in depleted gas fields and saline aquifers. Storage sites representing likely target formations for these two storage options have been selected: Rotliegend and Bunter sandstones. BEB Erdöl und Erdgas GmbH kindly provided information about an abandoned Rotliegend gas field for this case study.

1. Bunter Sandstone Aquifer Greifswalder Bodden

Concord Power Lubmin intends to build a gas-fired power station with an output of 1200 MW, at the site of the former nuclear power plant Lubmin. According to present plans the plant will emit about 3 Mt of CO_2 annually. The scenario composed for the GESTCO project assumes that CO_2 produced by this power plant can be injected into the Middle Bunter sandstone aquifer in the vicinity of the power station.

1.1 Aquifer Structure

The potential storage structure is relatively well known (Fig.1). It has been investigated by several deep wells and by seismic surveys on- and off-shore (Diener et al. 1992, Mayer et al., 1998). The site of the planned power station is located in a central position within this nearly 10 x 40 km large, NW–SE striking block of almost horizontal and barely faulted Bunter sandstone. From the Greifswalder Bodden area a gently inclined syncline is extending onshore, gradually turning into a gently dipping anticline in the area of Wolgast. These structures are bounded by fault zones (FZ): the NNW–SSE striking Freester FZ in the East, the Samtens FZ in the North and the 5 km wide complex FZ Möckow-Dargibell in the Southwest that includes the salt diapir Möckow. The observation of saline groundwater in the area of the FZ Möckow–Dargibell indicates vertical fault zone permeability (Mayer et al. 1998). This FZ may be a future safety risk that would require intensive risk assessment investigations. Thus we assume in the present scenario, that CO_2 will be injected in the eastern flank of the off-shore syncline.

The offshore part of the anticline has been explored by three wells and by extensive marine seismic surveys. Within the investigated area all of the four cycles of the Middle Bunter are present. The cycles begin with basal sandstone and end with a alternating succession of silt, sand and clay stone. Marked permeable sandstone beds occur in the basal parts of the three upper cycles (Detfurth-, Hardegsen- and Solling-Folge). These sandstone layers increase in thickness from SSW to NNE, reaching values between 20 and 40 m. The average effective porosity is between 20 and 25 %, exceptionally even 30 %. Measurements of capillary pressures indicate favourable transport properties of sandstones from the Detfurth- and Hardegsen-Folge. The permeability of these porous sandstones exceeds 500 mD and reaches maximum values of up to 2000 mD.

Depth of the Middle Bunter Sandstone near Lubmin

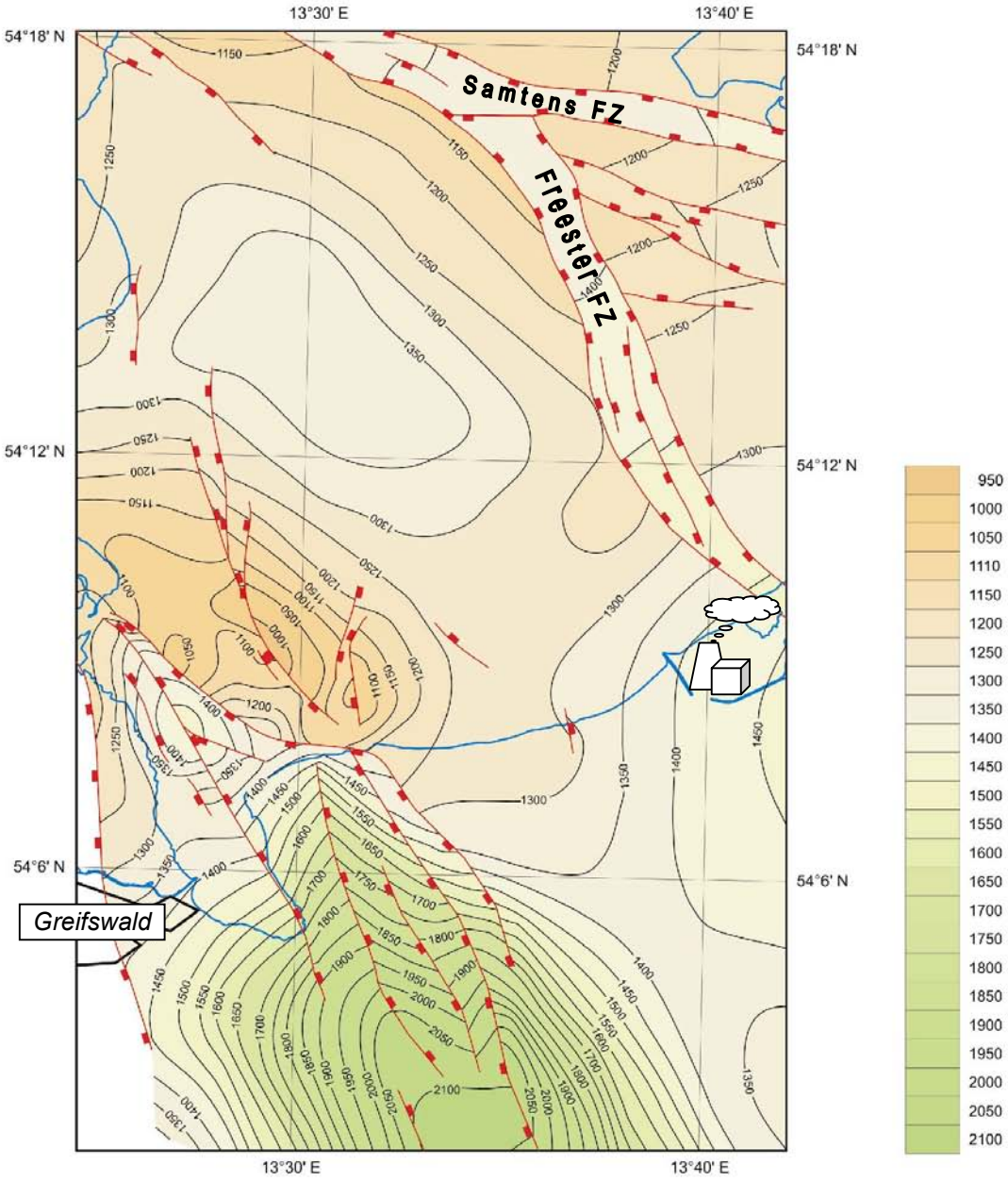

Isobath map of seismic S2 reflector

base of the Röt-Folge, top of the middle Bunter reservoir

shore line

site of Lubmin power plant

Figure 1. Topography of seismic reflector S2 that marks the top of the middle Bunter reservoir near Lubmin.

Assuming an average porosity of 22 vol.-% and a cumulative thickness of the sandstone layers of 80 m, the pore volume of the middle Bunter sandstones is 7.04 km³. If we further presume a final overall gas-saturation of 10 % and an average CO_2-density of 630 kg/m³ this aquifer could store 443 Mt of CO_2.

The Bunter formation waters contain 240 – 300 g/l of total dissolved solids at depths between 1200 and 1800 m. The salinity slightly decreases towards the north. On the island of Rügen, salinities of 147 to 228 g/l have been measured in the same stratigraphic position at depths between 1200 and 1300 m. Examples for the formation water composition and the composition of gases dissolved in the formation water are listed in the following tables 1 and 2.

Table 1. Analysis of Detfurth-Folge formation water from well Gt Ss 1/85 (Eichler 1987)

Cations [mg/l]	
Na^+	90283
K^+	624
Ca^{++}	13652
Mg^{++}	2206
NH_4^+	11
Fe^{++}	127
Anions [mg/l]	
Cl^-	171449
Br^-	1162
J^-	7.4
SO_4^{--}	566.2
density [kg/m³]	1185
salinity [g/l]	280.9
pH	5.1

Table 2. Composition of gases dissolved in formation water of well Gt Ss 1/85 (Eichler 1987

Gas component	CH_4	C_2H_6	N_2	O_2	CO_2	H_2	He
[Vol. %]	0.3	0.08	98.0	0.2	0.50	0.6	0.2

1.2 Numerical Simulations of subsurface CO_2 Injection

Numerical simulations were performed to study the effects of lateral extend and heterogeneity of the aquifer on storage capacity and efficiency. Another concern was the precipitation of halite from the high concentrated brines.

The TOUGH2 programme, version 2.0, of Pruess et al. (1999) has been used for numerical simulations of non-isothermal multi-phase and multi-component flow in porous and fractured media. Within this programme the EWASG module (Battistelli et al. 1997) calculates thermodynamic properties of water–NaCl–CO_2 mixtures. The pressure and temperature ranges of the original EWASG module of Battistelli et al. (1997) has been extended by Lorenz et al. (2001) in order to facilitate simulations at conditions appropriate for the underground storage of CO_2.

1.2.1 Modelling strategy for siliciclastic aquifers

Transport simulations are performed for the CO_2 injection phase – a short time scale of a few years. Geochemical reactions between groundwater, injected CO_2 and aquifer minerals are slow and are thus neglected in this phase. The reactivity of silicate minerals will have to be taken into account in considerations of long-term security. After the injection of CO_2 into closed structures, it can move slowly further with retarding velocity. For this phase transport can be neglected in geochemical models. In contrast to silicates, carbonates (and other salts) react much faster with carbonic acid solutions. The dissolution and precipitation of minerals can change the transport properties of carbonate aquifers. Thus coupled reactive transport simulations are required to simulate CO_2 injection into carbonate rocks. The Bunter sandstone however is essentially a quartz sandstone with iron oxide cement. Thus fast geochemical reactions are unlikely. The transport of dissolved salt and the precipitation of halite, which is known from the aquifer storage of natural gas, could effect the near well environment.

1.2.2 Reservoir characterisation

For modelling purposes the three cycles Detfurth-, Hardegsen- and Solling-Folge are divided into two lithologic units each, a lower sandstone unit and an upper alternating succession of sand, silt, and clay stones (Wechselfolgen). Average thickness values (Tab. 3) are calculated from the reported data of wells near Lubmin (Sauer 1976), Wusterhusen (Reinicke 1968, Sauer, 1979), Loissin (Becker and Jäger 1973, Beutler 1975), and within the Greifswalder Bodden (Reinicke 1970). Porosity values obtained from well tests are known from the wells Wusterhusen 1/67 and Lubmin 1/62 (Diener et al. 1992). For fine clastic rocks of the middle Bunter in Northwest Germany Schulz and Röhling (2000) report

a porosity of 11 to 17 %. Average sandstone to claystone abundances which were estimated from the lithostratigraphic inter-well correlation profiles (Reinicke 1970) are used to calculate weighted means for the porosities of the alternating successions (Wechselfolgen).

Permeability values for middle Bunter rocks have been reported from wells in the vicinity of Greifswald (Diener et al. 1992). These permeabilities were used to calculate a porosity–permeability relation, which allows estimating horizontal (arithmetic mean) and vertical permeability values (harmonic mean) from the porosities determined in the wells near Lubmin.

Table 3. Lithostratigraphic division and petrophysical parameter used in numerical simulations

lithostratigra-phic unit	thickness [m]	sandstone fraction [vol.-%]	porosity [vol.-%]	horizontal permeability [mD]	vertical permeability [mD]	density [kg/m³]
Solling Wechselfolge	9	50	17.1	160	1.79	2460
Solling sandstone	20	100	19	330	91.6	2430
Hardegsen Wechselfolge	41	33	16.6	152	1.55	2450
Hardegsen sandstone	21	100	22.5	450	128	2430
Detfurth Wechselfolge	47	10	16	55	1.13	2470
Detfurth sandstone	39	100	25	570	171	2430
Volprihausen Wechselfolge	135	0	14	0.1	0.05	

1.2.3 Numerical realisation, initial and boundary conditions

Fluid injection is simulated in a 3 x 3 km block of horizontal layers 177 m thick. In order to reduce the number of grid elements, an orthorhombic symmetry of the numerical model has been assumed. 40 kg/s of CO_2 are injected in the centre of the basal Detfurth sandstone layer in a single vertical injection well (numerical element volume 35100 m³).

Constant pressure, temperature and salinity gradients have been used as initial conditions. Pressure Gradients in the Bunter are in the range of 10.5 to 10.9 kPa/m (Beutler, 1975). The average temperature gradient in the wells Loissin 1/70 and Wusterhusen 1/67 is 35 K/km (Beutler, 1975; Reinicke, 1968). The mean annual air temperature at the surface is 8°C. At the model base a constant temperature boundary is provided. Heat exchange with the overlying strata is simulated using a semi-infinite conductive layer.

The salinity of the Bunter formation water in a well near Wolgast is about 250 g/l, slightly below halite saturation. It increases with depth at a gradient of about 80 (g/l)/km (Becker and Lenz, 1992).

The lower and upper model boundaries were assumed to be impermeable (fine clastic Lower Bunter and Volpriehausen Wechselfolge below – and Röt claystones above of the reservoir). Lateral boundary conditions permit fluid flow to the surrounding aquifer of a) infinite extend or b) 10x40 km extend. The latter assumption is rather conservative, assuming that the block boundary fault zones within the Greifswalder Bodden are impermeable. The observation of saline groundwater in the area of the Störungszone Möckow Dargibell indicates vertical fault zone permeability at least (Mayer et al. 1998).

1.2.4 Results

Three models with different aquifer properties are simulated:

1. homogeneous infinite aquifer, with anisotropic permeability
2. homogeneous finite aquifer, with anisotropic permeability
3. heterogeneous finite aquifer, with anisotropic permeability

The simulated spreading of CO_2 injected into the well permeable sandstone of the Detfurth-Folge is initially in lateral direction. However, upwards migration through the less permeable Wechselfolge successively opens a two-phase flow connection to the hanging higher sandstone units. As the gas saturation above the injection point increases the vertical flow soon exceeds the horizontal spreading within the Detfurth sandstone. The radius of the gas bubble around the injection point decreases again and a rather narrow chimney of high gas saturation and relative permeability facilitates the ascent of the injected CO_2 and its spreading beneath the Röt caprock. The gas accumulates within the Solling sandstone, reaching gas saturation values of up to 65 vol. % (Fig. 2).

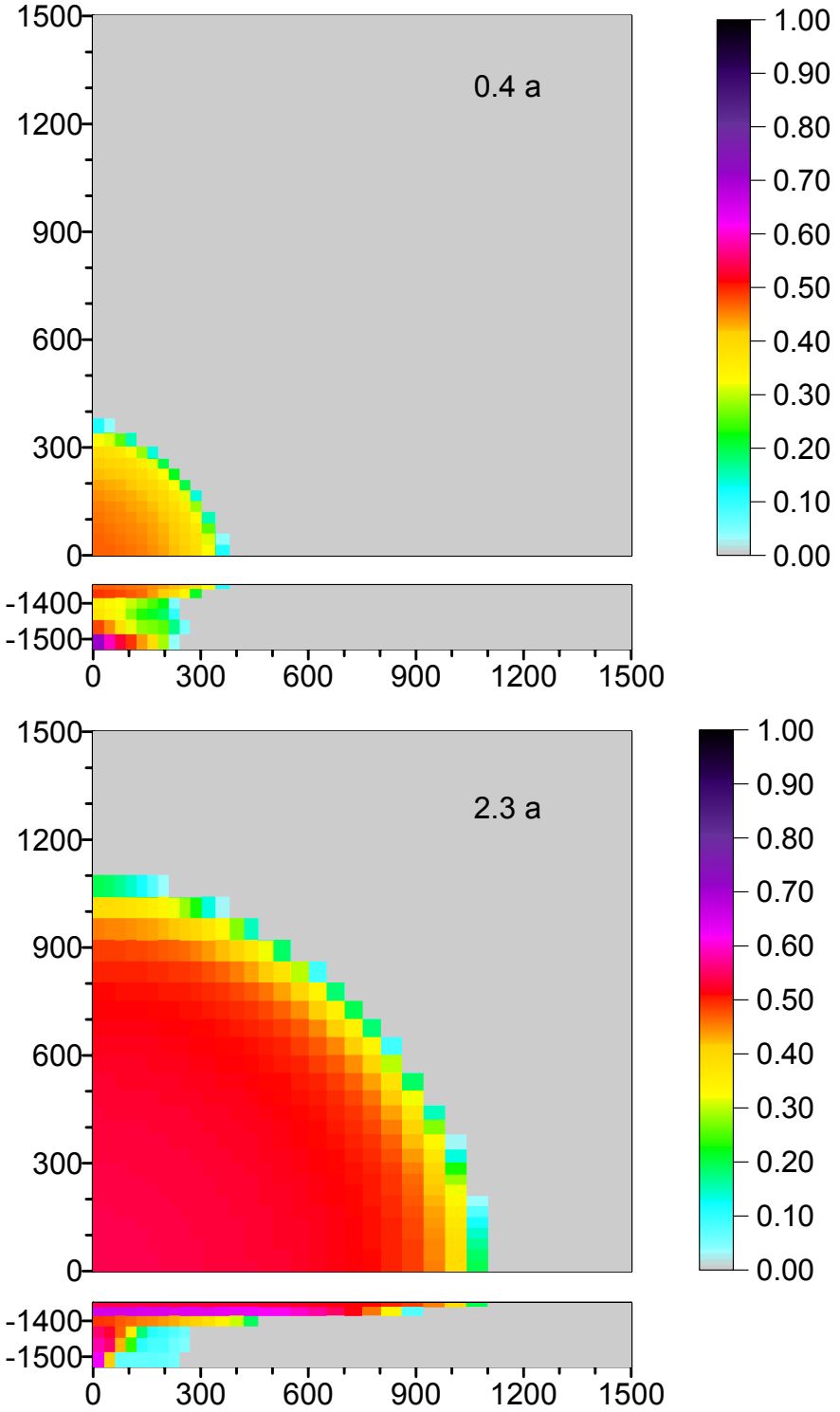

Figure 2. Horizontal maps (Solling Wechselfolge) and vertical profiles of the gas saturation, after 0.4 years of CO_2 injection and at the end of the simulated injection period (infinite homogeneous aquifer).

Initially the pressure around the injection well increases. With the progressive displacement of formation water and the expansion of the gas phase pressures decrease again. At the given injection rate, the pressure increase around the injection well is only 0.2 MPa. At the

top of the reservoir the pressure increase is stronger: about 0.6 MPa within the first two months, slightly increasing up to a maximum of 0.64 MPa which is reached after about 200 days of CO_2 injection, followed by a gentle decline again. The injection induced pressure exceeds the initial formation pressure not more than about 4.6 %. Thus the chances for formation damage due to geomechanical reactions of the reservoir or cap rocks are probably low.

The heterogeneous model has been set up in order to study the effects of permeability variability on the CO_2 migration within the aquifer. The measured permeability values of the Bunter sandstone samples from wells of the Greifswald area are log-normally distributed. The uniform permeability values of the six reservoir layers have been modified with random log-normal distributed permeability modification factors (Fig. 3). The standard deviation of these factors is according to the measured permeability variation. Most of the values are within a range of two orders of magnitude.

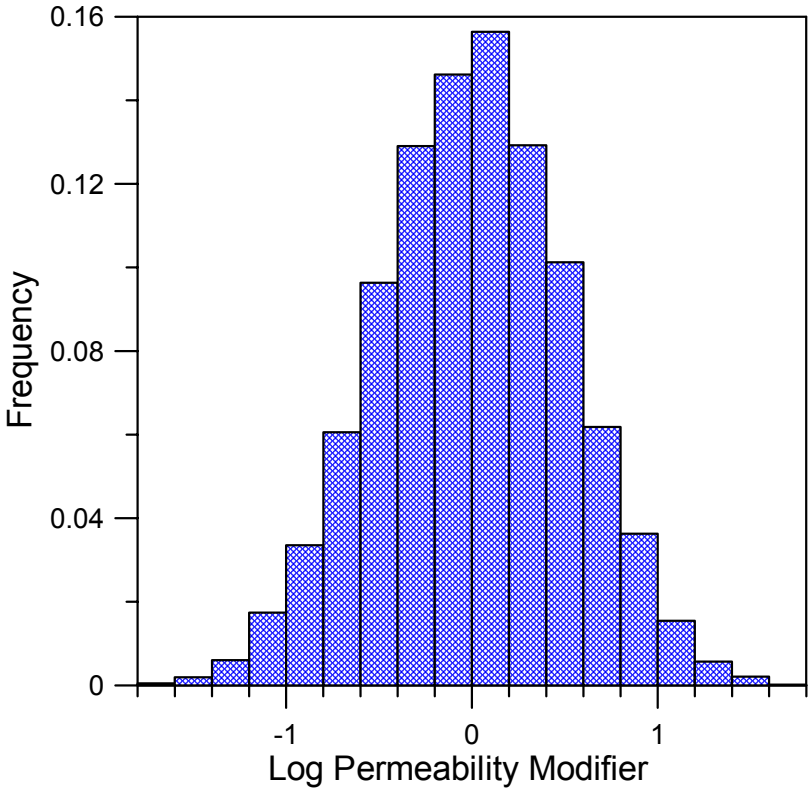

Figure 3. Simulated log-normal distributed permeability variation used to generate the heterogeneous model.

The numerical realisation of the permeability distribution within the six layers of the model is shown in Figure 4.

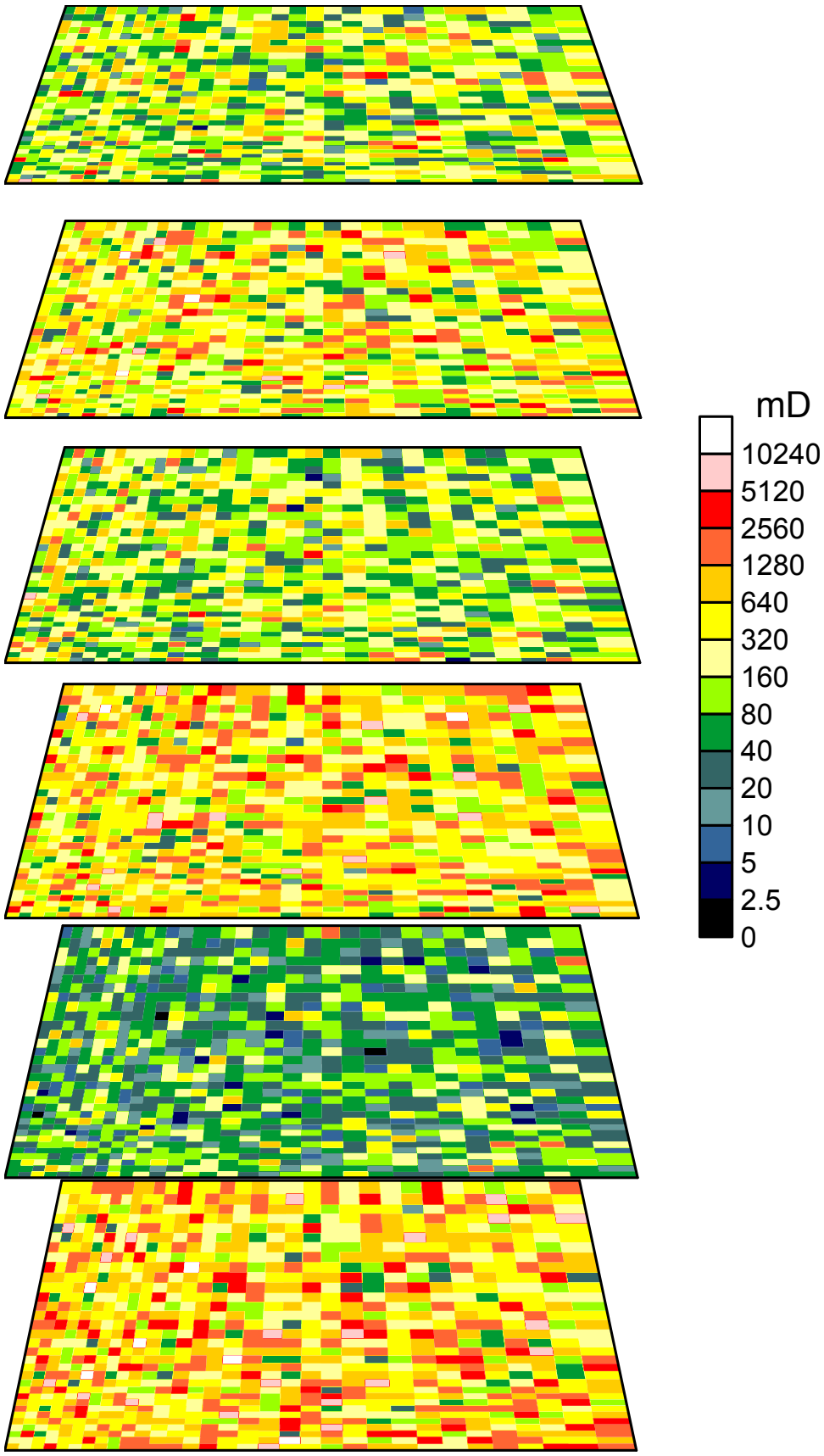

Figure 4. Modelled horizontal permeability distribution in six model layers. The lower left corner is the central fluid injection point in the model of orthorhombic symmetry.

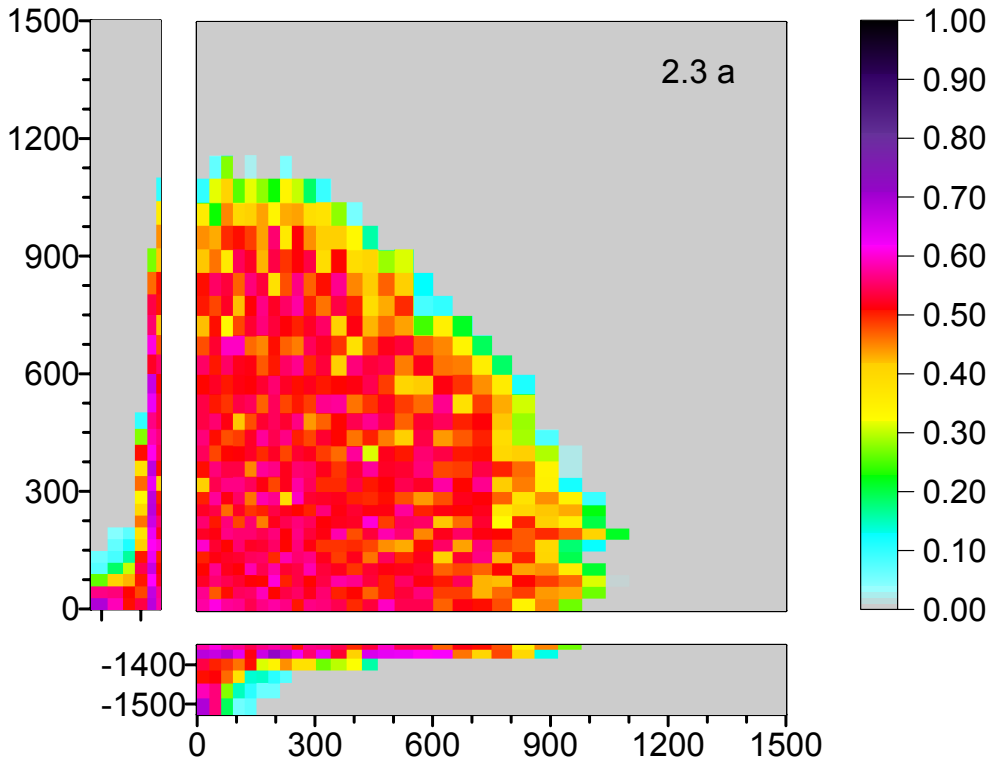

Figure 5. Horizontal map (Solling Wechselfolge) and vertical profile of the gas saturation at the end of the simulated injection period (finite heterogeneous aquifer).

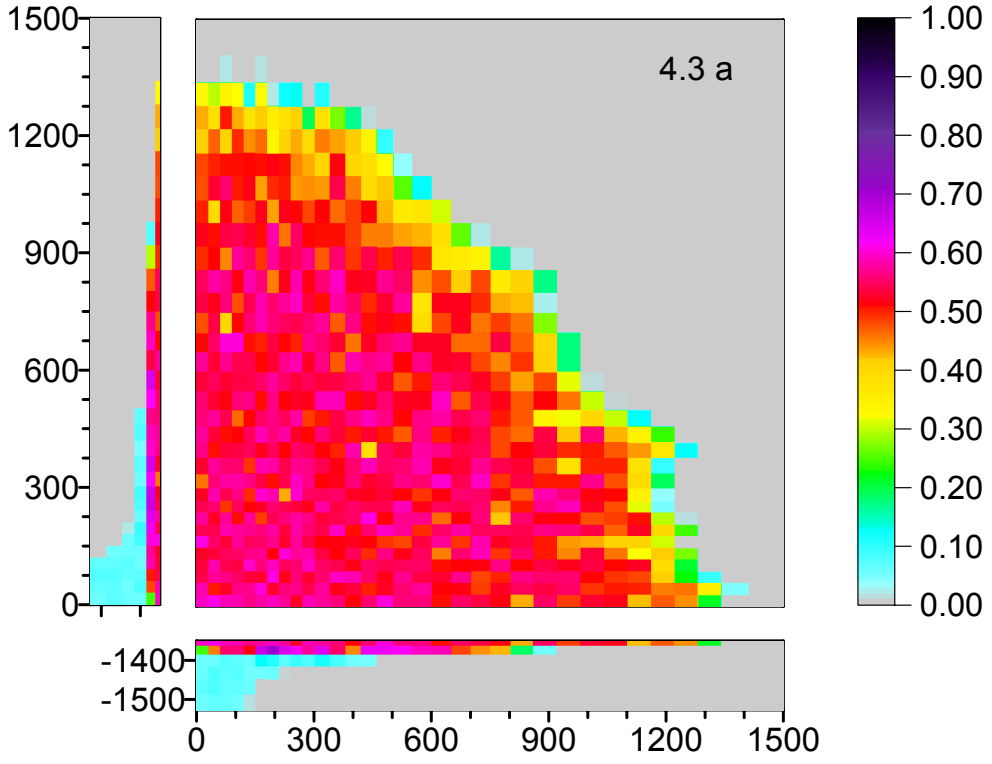

Figure 6. Horizontal map (Solling Wechselfolge) and vertical profiles of the gas at the end of the simulated time period (boundary elements reached).

In accordance to the homogeneous models injection has been simulated for 2.3 years (4.8 Mt of CO_2 injected in total). The randomly distributed permeability does not result in a gas phase distribution much different from the homogeneous models (figs. 5, 6). Along the flow paths of the expanding gas phase the effects of more or less permeable elements level out. The amplitude of fingering of the expanding gas front is in the order of about 100 m.

The ratio of the mass of injected CO_2 to the mass of CO_2 that could fill the entire pore volume (100 vol.-% gas saturation) of the reservoir part covered by the CO_2 umbrella is used as a measure of sweep efficiency. With increasing radius of the gas bearing area the volume of the missed aquifer portion increases asymptotically towards an efficiency of about 0.09 at the end of the injection phase (Fig. 7).

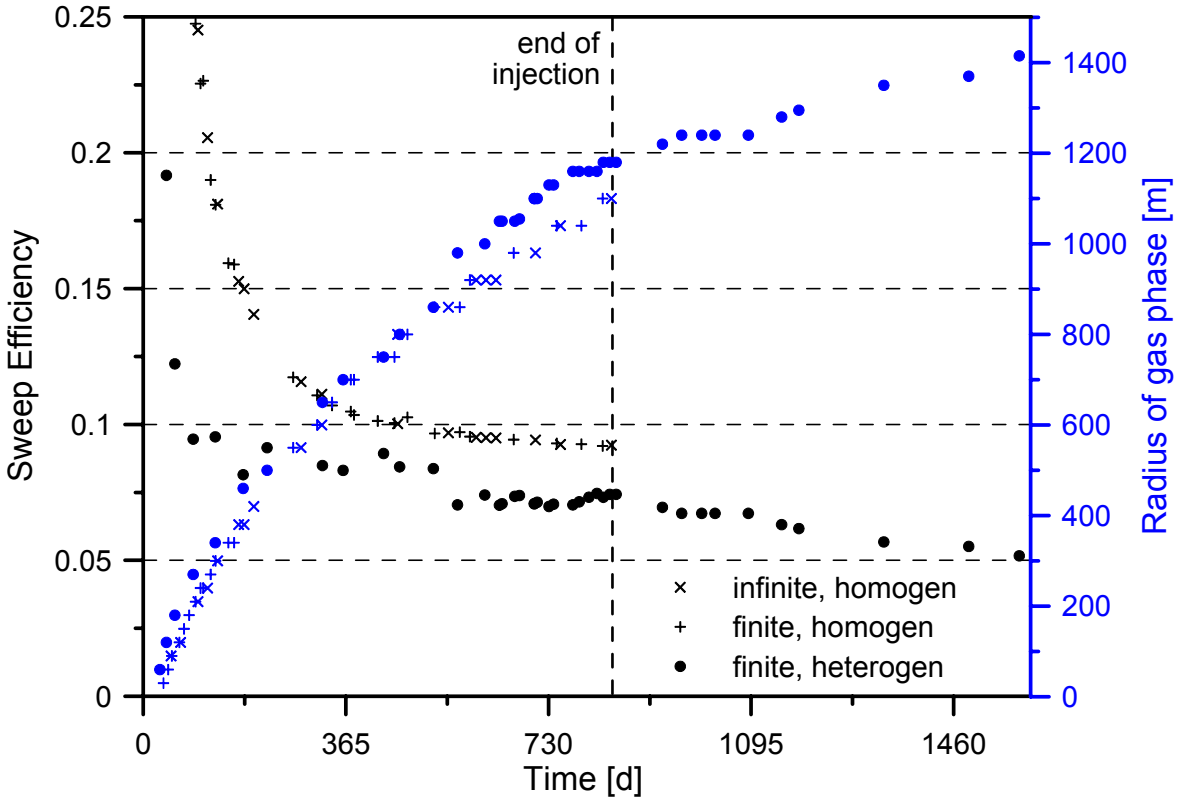

Figure 7. Temporal variation of sweep efficiency and gas phase radius during 2.3 years of injection, followed by a 2 year post-injection period (heterogen model only).

For the heterogeneous model the size of the injection area has been calculated as a sphere with the diameter of the maximum radius of the gas phase. This way the reservoir volume between the gas fingers is taken into account to calculate more realistic storage efficiencies, which are lower than those of the homogeneous models that yield a spherical two-phase area. Taking into account the post-injection expansion, the storage efficiency decreases further to 0.05 or less. A future minimum value can be expected, when the

progressive dissolution of CO_2 will compensate the gas expansion and the bubble will start to shrink again. The simulated radius/efficiency relation can be used to derive efficiency limits and to plan the spacing of vertical injection wells.

Little difference exists in the way the injected CO_2 spreads between the finite and infinite model. Only close to model boundary where fluid pressures are below the initial values, due to forced convection of the liquid phase flowing downward, the two models differ (fig. 8). While the infinite aquifer model keeps the boundary pressure constant, the fluid pressure in the finite boundary elements drops below the initial values, due to the participation of the boundary elements in the fluid convection. In the finite model only 0.79 vol.-‰ of the pore volume is occupied by the gaseous phase. The models are likely to differ in post-injection pressure relaxation and reservoir pressure gradients. Two years after the end of injection the horizontal fluid pressure at the reservoir top has become much smaller, but the gas phase is still expanding laterally. At that time the gas phase has reached the model boundary elements, so that no final steady state can be simulated.

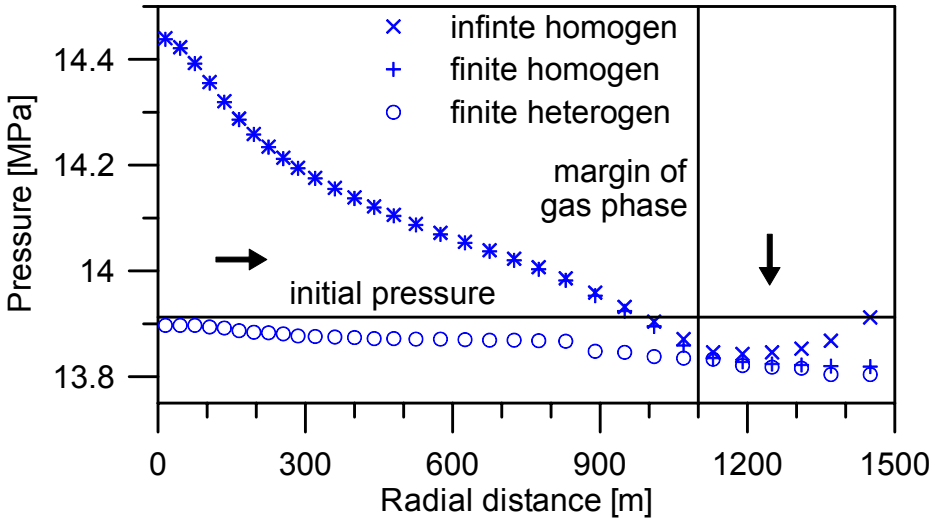

Figure 8. Simulated fluid pressure at the top of the reservoir, at the end of CO_2 injection period (homogeneous models) and after two years of pressure relaxation (heterogeneous model). Arrows indicate the principle directions of fluid flow.

The extrapolation of the storage capacity obtained in the 3x3 km model to the entire fault bounded block of about 10 x 40 Km (on and offshore as well) yields a total storage capacity of about 250 Mt of CO_2. This estimate is based on a simple injection pattern with low efficiency and low over pressure (homogeneous model). The irregular front of the gas phase only slightly increases the amount of CO_2 that dissolves in the formation water, compared to the homogeneous model. After about one year of injection both models do not

differ in this respect any more (fig. 9). The fraction of CO_2 that dissolves during the injection phase is about 13 wt.-%. In the post injection expansion phase further CO_2 is dissolved.

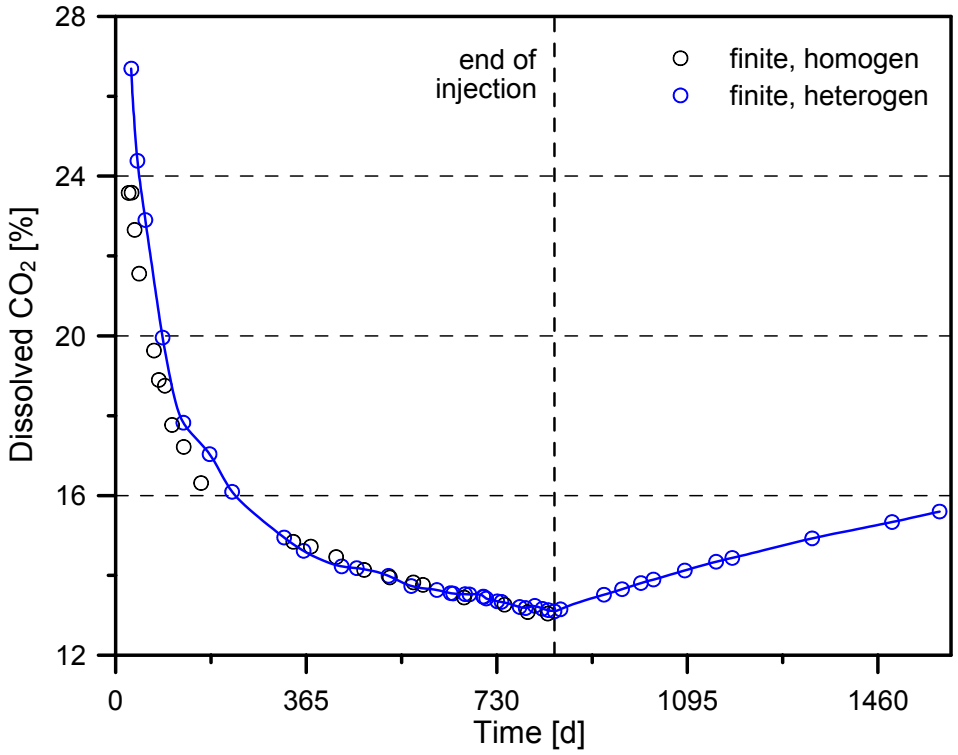

Figure 9. Temporal evolution of the fraction of CO_2 in solution

Formation water will evaporate into the injected dry CO_2-rich gas phase. Thus the concentrations of solids dissolved in the formation water increase and eventually the precipitation of salt begins. According to the dimensions of the grid elements used in these simulations, salt precipitation from the highly concentrated brines will start early, after about six month of CO_2 injection. Salt precipitation is limited to the grid element of CO_2 injection however (30x30x39 m). According to the constant injection rates, the total amount of salt precipitated increases linearly, until about 7.3 vol.-% of the original pore space is filled with halite. The absolute porosity decrease from 25 to 23.2 vol.-% has no marked effect on the pressure necessary to maintain constant injection rates.

The permeability reduction due to salt precipitation is calculated using a tubes-in-series model (Verma and Pruess 1988, quoted in Pruess et al. 1999), which yields a 15 % permeability reduction for the maximum amount of salt precipitation (fig. 10). The shape of the permeability reduction curve is however dependant on the actual pore size distribution and geometry. It should be determined experimentally on rock samples for better quantification of likely near-well permeability reduction.

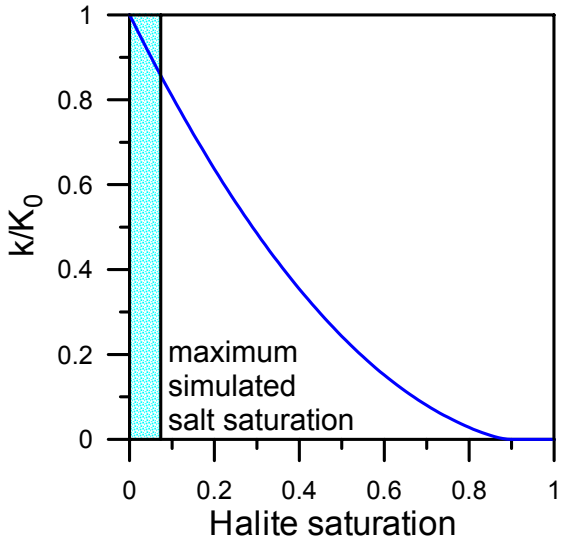

Figure 10. Relation of salt saturation and permeability calculated for the tubes-in-series pore space model, used in the present simulations.

After the end of injection, CO_2 rises rapidly and formation water re-enters the injection element and dissolved precipitated salt again. However the salt concentrations of the water flushing from adjacent elements soon reach halite saturation so that not all of the salt can be dissolved again (fig. 11). In practice this means that salt precipitation from the formation water is irreversible and could require freshwater flushing if the permeability would drop too low.

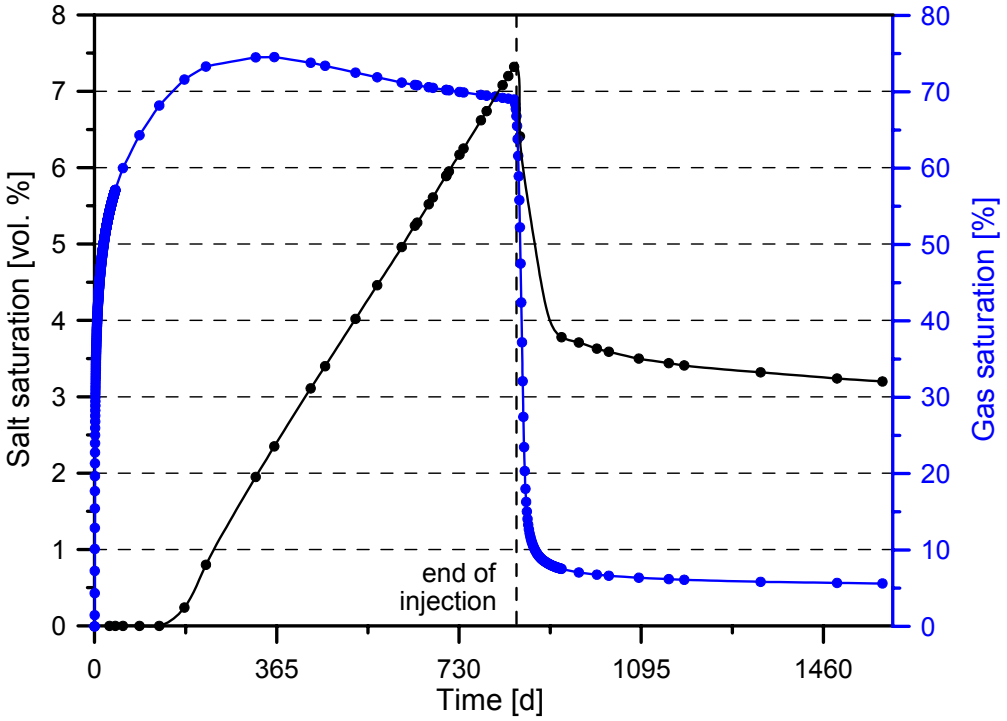

Figure 11. Temporal evolution of gas and salt saturation of the pore space within the element of CO_2 injection.

1.2.5 Critique and Limitations

The results of the present simulations help to understand and predict likely processes of CO_2 injection into the Bunter sandstone in the Greifswalder Bodden area.

Further reservoir simulations should attempt

- to calculate larger models and longer injection as well as relaxation times;
- the optimisation of injection patterns (several injection wells) and timing in order to increase the storage efficiency;
- to use amore detailed stratigraphy and permeability modifications according to sedimentary facies models and reservoir analogues of the Bunter sandstone;
- to consider inclination of the reservoir rocks.

In order to perform predictive reservoir modelling additional information is required. Experiments on cores are necessary to quantify relations between gas saturation and relative permeability or capillary pressure and the reduction of porosity and permeability due to salt precipitation. Hydrogeological tests are required to get a better estimate of the size of the aquifer and the permeability of the block boundary fault zones.

2 Gas field Alfeld-Elze and Hildesheimer Wald

The former gas field within the concessions Alfeld-Elze and Hildesheimer Wald covers the area of the city of Elze (population ~ 6000) and adjacent villages. It is connected by a 20 cm diameter pipeline to the regional network. A storage capacity of 8 Mt CO_2 is calculated from the amount of natural gas produced from this reservoir, mainly from the wells in the concession Alfeld-Elze. Power stations and cement works in Hannover, about 35 km north of Elze emit several million tons of CO_2 annually. Thus, the field would only be able to take up the emissions of one of the power plants for a period of 5 to 10 a. Capture and collection of emissions from different sites in the region in order to pipe them to a more extensive storage site would be a longer lasting storage option for power plants in Hannover. However the gas field could provide an interesting storage option for a nearby sugar factory. The most energy intensive process in sugar generation from sugar beets is the evaporation of the beets water content. The Nordstemmen sugar factory produces about 125 kt of sugar annually from 780 kt beets which are processed in about 80 days. Natural gas- and coal-fired pans are used to evaporate the water from the beets. The average primary energy consumption to process one ton of beets is 300 kWh (Wirtschaftliche Vereinigung Zucker e.V. 2001). Thus the CO_2 emissions from a sugar factory of the size of that in Nordstemmen would be about 70 kt per season, requiring a CO_2 injectivity of about 1000 t of CO_2 per day. In the beet processing season 2001 6000 t of coal and 16 Mm^3 of gas were burned, releasing about 50 kt of CO_2. This is about 7.2 kg/s. After the beet processing season the injection wells could be used to take up some CO_2 from other sources. Local medium size industry (foundry at Elze, paper mill in Alfeld) does not emit much CO_2 tough. Only a fraction of the CO_2 emitted by power plants near Hannover could be injected. The storage capacity would be sufficient for about 22 a of CO_2 injection at 1 kt/d.

The well Nordstemmen Z1 that has reached the flank of the closure of the gas field was drilled only about 4 km away from the sugar factory. A short pipeline, crossing the river Leine, could be built or a well of extended reach could be drilled on site of the factory to inject the CO_2. Due to the close distance between sugar factory and the gas field, CO_2 could be compressed sufficiently for injection at the separation plant already.

2.1 Gas field structure

The Rotliegend gas field Alfeld-Elze and Hildesheimer Wald has produced 1.86 x 10^9 normal m^3 of natural gas from 1972 until 1996. The gas reservoir is within a thick upper Rotliegend sandstone, unconformably overlying carboniferous basement rocks. The upper Rotliegend sedimentation in the continental North German Basin is characterised by

climate controlled regressive, coarsening upwards cycles (Gralla et al. 1991). Transgressive fine clastic sediments at the base of each cycle did not develop in the Rotliegend Hauptsandstein at the southern basin margin near Elze. There the continuous sedimentation of fluvial sand created a sandstone formation of 100 to 250 m thickness that forms the gas Reservoir. Only in the uppermost part of the Hannover Formation cyclic sedimentation has led to an alternating succession of fine and coarse clastic sediments, the Rotliegend Wechselfolge. The Wechselfolge consists of clay stones, marl, silt, fine-, and medium-grained sandstones. Due to the exogenetic control of the sedimentation pattern, the cycles are laterally extensive and can be correlated over long distances (Schröder et al. 1995). The clay stones of the 30 to 50 m thick Wechselfolge are the cap rocks of the gas reservoir. The lower Zechstein Basiskonglomerat is not present and Kupferschiefer up to one meter thickness has been found in a few wells only. In most of the wells The Zechstein 1 cycle begins with about 9 m of Zechsteinkalk (dolomitic limestone), followed by an average of 48 m of Werraanhydrit (anhydrite, partlly dolomitic and gypsum). The lower Zechstein 2 cycle consists of about 13 m of Staßfurtkarbonat (Ca2, anhydritic and dolomitic limestone) and about 3 m of Basalanhydrit. The reservoir properties of the Staßfurtkarbonat are strongly facies dependant. The limestone below Elze has been deposited in a transitional position between lower slope and basin, which is characterised by fine-grained, low permeable rocks (Steinhoff 1995). The rock salt of the Staßfurt cycle 25 – 170 m thick covers the lower Zechstein succession that is gas bearing up to the Staßfurtkarbonat. The Hauptsandstein Reservoir forms a domal closure with some suspected faults displacing the south-eastern parts of the structure (Kockel 1984; Bachmann and Mutterlose, 1987). Large variations of Hauptsandstein thickness (93 to > 470 m) between different wells may be a result of synsedimentary faulting and/or palaeotopography.

The gas field is part of the of the anticlinal Leinetal structure (fig. 12). Zechstein salts have been squeezed into thrust zones during compression and inversion in the Coniacian and Santonian. Leaching of the top of the salt wedge commenced in the Mastrichtian, leading to the collapse of the overlying Bunter sandstone (Jordan and Kockel 1991). Continuous subsidence is indicated by the thickness of Quaternary sediments and the morphology of the Holocene Leine gravel deposits (Lüttig 1960).

The top of the gentle dipping antclinal structure has been drilled in the well Alfeld-Elze Z3 at about 1300 m depth. Along the axis of the anticline a fault with about 200 m of vertical displacement is suspected (fig. 13).

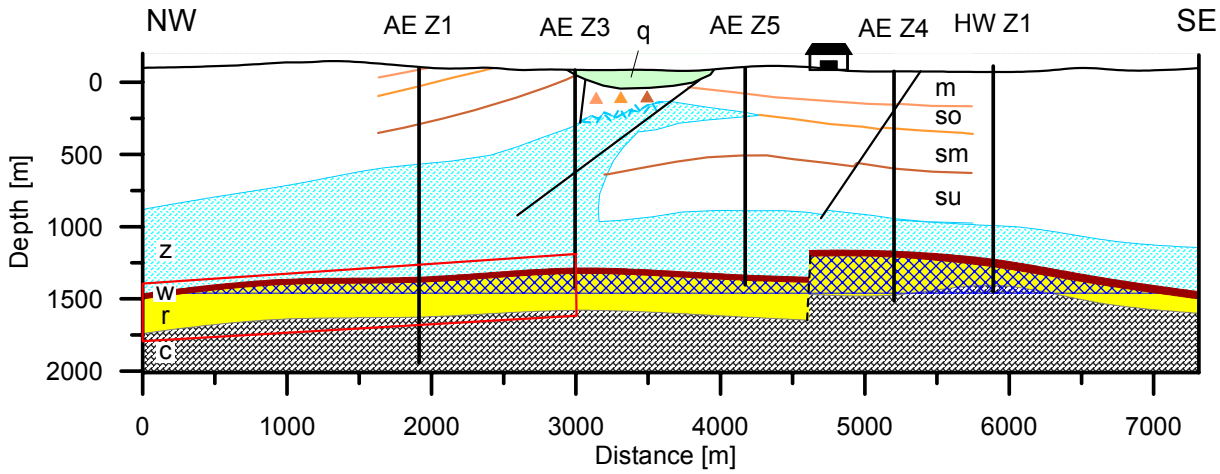

Figure 12. Geological profile of the gas field Alfeld-Elze and the Leinetal structure. Stratigraphic divisions: Carboniferous (c), Rotliegend Hauptsandstein (r), Rotliegend Wechselfolge (w), Zechstein evaporites (z), lower, middle and upper Buntsandstein (su, sm, so), Muschelkalk (m) and Quaternary (q). The blue hatched area marks the gas bearing part of the reservoir. Triangles indicate collapsed Bunter rocks due to subrosion. The hut indicates the position of Elze. The red parallelogram indicates the dimensions of the numerical realisation. Composite geological profile based on data of Jordan and Kockel (1991), Kockel (1984), Sedlacek und Stancu-Kristoff (1993).

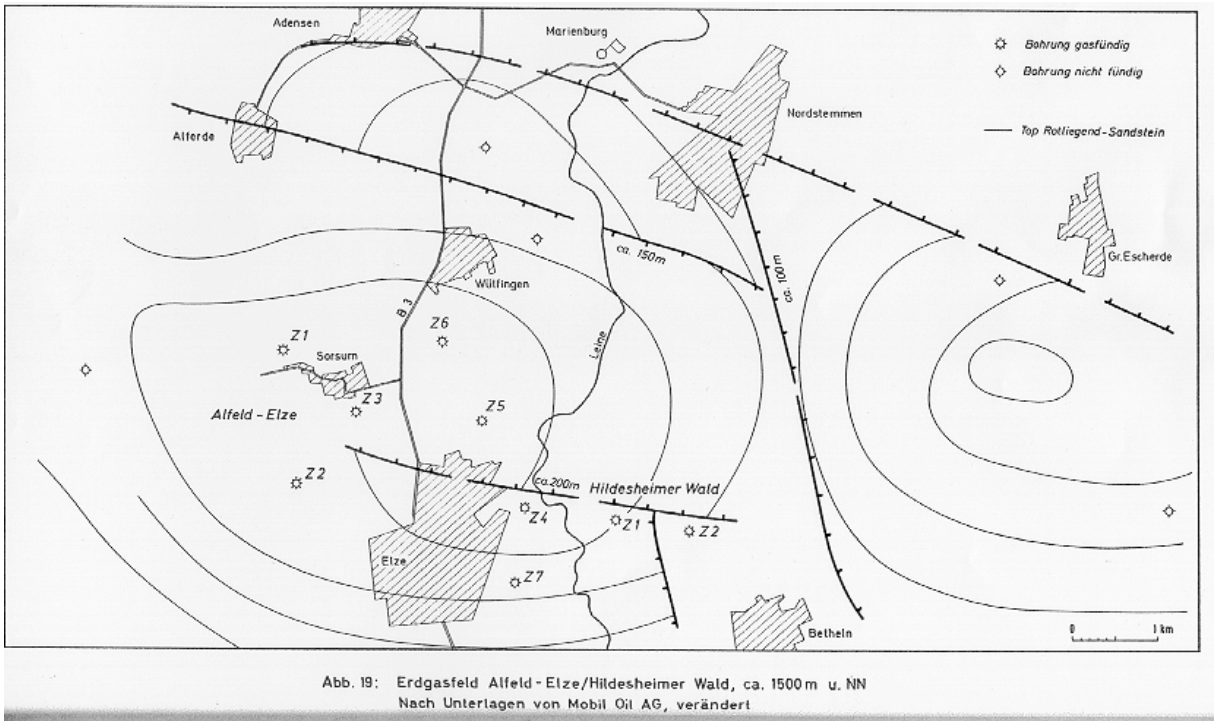

Figure 13. Contour map of the gas field Alfeld-Elze; copy from Bachmann and Mutterlose (1987)

2.2 Numerical Simulations of subsurface CO_2 Injection

2.2.1 Reservoir characterisation

The numerical model comprises a succession of carboniferous claystones and sandstones, the Rotliegend Hauptsandstein reservoir and the Rotliegend Wechselfolge caprock. The lower Zechstein anhydrite and dolomitic limestones forming a potential reserve aquifer is also included in the model. The Staßfurt salt is the upper boundary for the numerical model.

While the Hauptsandstein rocks have been cored and a large number of porosity, permeability, and density values have been obtained from the core samples, only few values have been obtained from the hanging and lying formations. Other petrophysical parameters have not been measured. They had to be estimated from literature data of comparable formations or rock types (tab. 4).

Different methods are appropriate for up-scaling of sample-scale petrophysical parameters to model grid dimensions (Haase 1997). Weighted arithmetic means of the volumetric properties density and porosity are used to calculate mean values. Up-sacaling of permeability, which is the most influential parameter effecting fluid flow, has been treated differentially: The permeability and porosity measurements of the Rotliegend Wechselfolge show a bimodal distribution, probably representing fine- and medium-grained sandstones, which have been preferentially sampled. No porosity/permeability measurements were made on Wechselfolge claystones. For the stratified laterally extensive Wechselfolge the weighted arithmetic mean represents layer-parallel permeability, while the harmonic mean is used to calculate flow perpendicular to the layering.

Porosity values of Hauptsandstein core samples show a normal distribution with an arithmetic mean of 6.7 vol.-% (fig. 14). Average formation porosity values are higher, due to the fractured nature of the reservoir. A weighted arithmetic mean of 9.3 vol.-% is used in the simulations. Spacing, width, and orientation of fractures in the reservoir are not known. The average spacing of sub-vertical fractures in an East German Rotliegend reservoir (1.6 to 3.6 m, Ziegenhardt et al. 1977) is much less than the numerical grid block length of 20 m. Thus, the fractured reservoir can be treated as a homogeneous medium. The core porosity-permeability distribution has been used for up-scaling of the log-normally distributed core permeability values, yielding an average formation permeability of 0.13 mD. The average field to core permeability and porosity ratios of the Hauptsandstein have been used for up-scaling of core permeability and porosity values for the siliciclastic rocks

adjacent to the Hauptsandstein. Anhydrite has precipitated in fractures of the hanging Zechstein rocks. Permeability and porosity values for these rocks have been estimated.

Table 4. Litho-stratigraphy of wells Alfeld-Elze Z1 und Z3. Mean values and (ranges) of petrophysical parameters.

Lithostrati-graphy	Thickness / Lithology	Permeability =	Permeability ⊥	Porosity	Rock Matrix Density	Thermal Conduc-tivity, wet, geometric Ø	Specific Heat Capacity, dry (e)	Thermal conductivity, dry (e)	Klinkenberg Parameter	Residual Water Saturation
Unit	[m]	[mD]	[mD]	[%]	[kg/m^3]	[W/mK]	[J/kgK]	[W/mK]	[Pa^{-1}]	
Z2 Karbo-nat	13	0.1 (e)		4 (tight – 8.1)	2575 (e).	4.59	850	5		
Z1 Anhydrit	48	0.001 (e)		0.1 (e)	2800 (e).	5.228	900	5.3		
Z1 Karbo-nat	9	0.1 (e)		0.6 (1)	2575 (e)	4.937	850	5		
Rotliegend Tonstein Wechsel-folge 36 m	MS	0.855 (0.02 – 1)	0.359	4.2 (2.7 – 3.3)	2720 (2690 – 2740)	1.901	825	2		.32 (2)
	FS	0.0126 (0.001 – 0.01)	0.0116	1.96 (0.9 – 2.1)	2720 (2690 – 2740)	1.953	825	2		.5 (2)
	clay stone	0.0001 (0.62 – 50 x 10^{-6}) (3) <0.00123 (2)	0.00005	0.98 (0.5 – 0.9) (3) 3.1 (2)	2750 (e)	2.368	750	2.4	2670000 calculated	.6 (2)
Rotliegend Sandstein	**244**	**.13 (0.0155 – 1.55)**		**9.3 (1 – 13)**	**2655 (2660 – 2700)**	**1.788**	**825**	**2**		**0.18 minimum well log value**
Namur C > 220 m	sand stone	0.15 (0.001 – 8)		10	2770 (2700 – 2800)	2.358	750	2.4		0.125 minimum well log value
	clay stone	0.00007 (<0.1 – 75.7 x 10^{-6}) (3)		1.28 (0.3 – 1.9) (3)	2800 (e)	1.773	825	2	3540000 calculated	.6 (2)
Carbo-niferous	geo. ∅	0.00324		3.58	2785	2.1	788	2.2		

(1) Steinhoff (1995), (2) Rudolph et al. (1972), (3) Schlömer und Krooss, (e) estimate

Tabulated values of thermal conductivities and heat capacities of common minerals and rock types (e.g. Clauser and Huenges 1995) have been used in the numerical models. Fluid saturated thermal conductivities have been calculated as weighted geometric means. Uniform values for thermal expansivity (10^{-6} K^{-1}) and pore compressibility (10^{-9} Pa^{-1}) have

been assigned to all rock types. A residual gas saturation of 0.05 (Wustrow Sandstone sample measured by Winter and Meyn 1997) has been used in relative permeability functions.

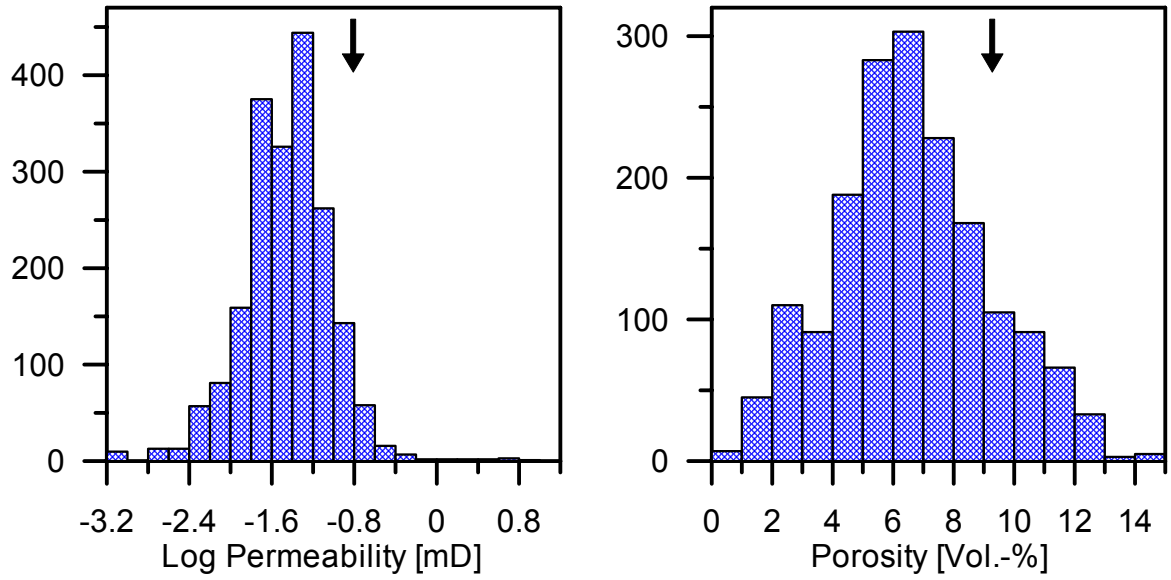

Figure 14. Measurements of Rotliegend Hauptsandstein core samples. Arrows indicate estimated average formation values used in the numerical models.

2.2.2 Numerical realisation, initial and boundary conditions

The numerical model represents mainly the western part of the gas field, the concession Alfeld-Elze. A 2.5-D rotational symmetric model has been chosen for the numerical realisation. A radial cross section of the model is indicated by the red rhomboid in the geological profile. The radius of the cylindrical model is 3000 m the vertical thickness is 411 m. A constant radial inclination of the top and basal surface of 3.46° represents the domal structure of the reservoir.

The >25 m thick Z2 Staßfurt salt is taken as upper, impermeable boundary. 65 m of alternating carboniferous claystones and sandstones are taken as lower boundary of the Rotliegend sandstone reservoir. The top and bottom boundaries are "no flux" boundaries. The lateral boundary has been assigned quasi constant thermodynamic conditions by large volume ring elements of 10 km outer radius.

The average initial water saturation in the reservoir was 46.6 vol.-%. The pore volume of the gas bearing reservoir rock above -1480 m depth is 58.8 x 10^6 m^3. Under average initial reservoir conditions at a depth of -1450 m (17.5 MPa, 50 °C) the produced N_2-bearing natural gas had occupied a volume of about 7.5 x 10^6 m^3. Gas production came to an end when the co-production of formation water exceeded economical limits. Thus, a final gas

saturation of about 40.7 % is assumed for the reservoir. Initial pressure and temperature conditions in the reservoir indicate a hydrostatic pressure gradient and a temperature gradient of 30 K/km (fig. 15). These conditions have been used for single phase fluid domains.

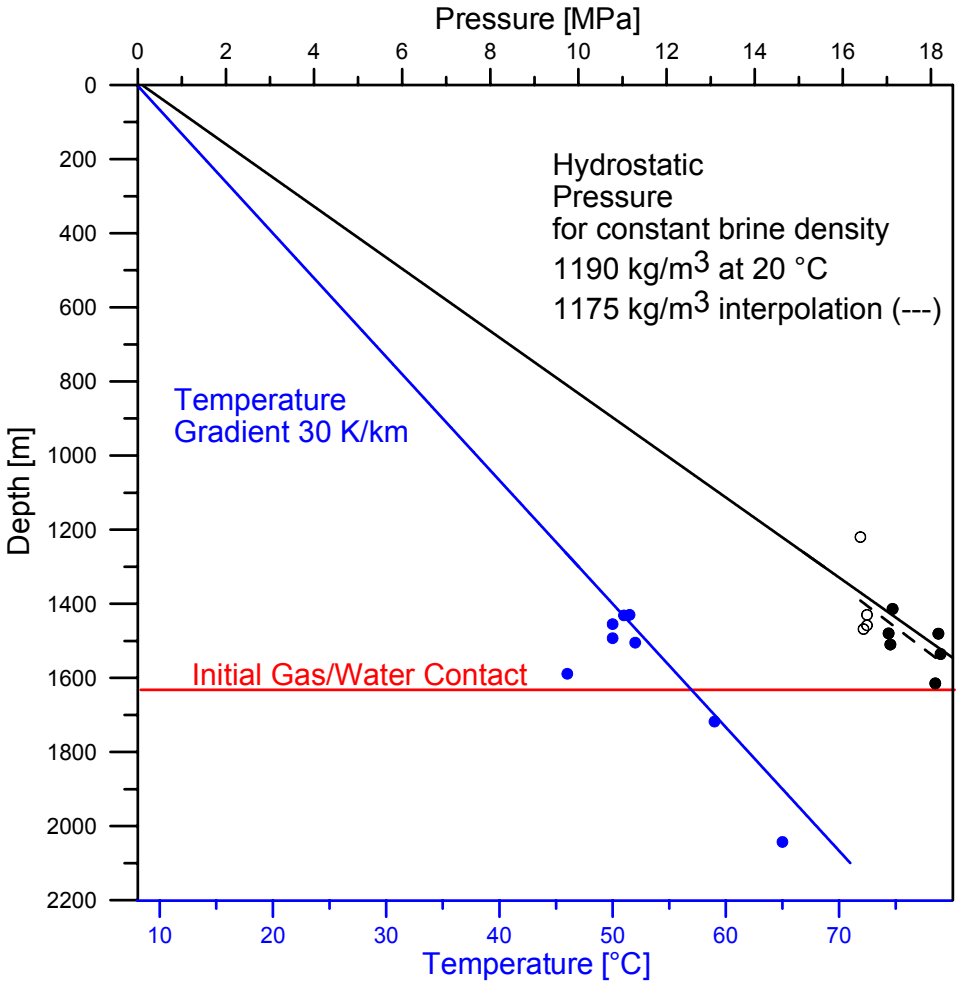

Figure 15. Measured initial pressure and temperature conditions in the gas field Alfeld-Elze / Hildesheimer Wald.

Adequate representation of CO_2 dissolution in formation water was difficult to realise in the numerical model. In nature the CO_2 concentration in solution will be proportional to the CO_2 partial pressure (Henry's law). The numerical model can not take into account the partial pressure of the natural gas in the reservoir. Initial fluid pressure conditions in the gas-bearing part of the storage formation can be realised as 1) partial pressure of CO_2 or 2) hydraulic pressure within the reservoir.

1) Fluid pressure = pCO_2 (Simulations Elze03)

The CO_2 partial pressure is taken as initial pressure within the gas-bearing part of the reservoir. The initial CO_2 concentration in the formation water can be modelled realistically

this way. However the reservoir's natural gas will be "evacuated" yielding space for CO_2 and exaggerated pressure gradients. This will increase storage capacity and CO_2-flow velocities into the under-pressured reservoir. Unrealistic pressure gradients result in exaggerated CO_2 expansion and hence cooling below the valid temperature range of the equations of state, causing programme termination after about 9 month of CO_2 injection. Further, the increase of CO_2 partial pressure beyond values expected by mixing of CO_2 and natural gas will additionally increase the proportion of CO_2 storage in the formation water.

2) Fluid pressure = hydraulic reservoir pressure (Simulation Elze04)
It is assumed that the pressure distribution within the reservoir is equal to the formation pressure at the end of the gas production: hydrostatic – 1.5 MPa production induced pressure drop (wells Hildesheimer Wald 1 and 2, Sedlacek and Stancu-Kristoff (1993)). In this case the initial CO_2 concentration in the formation water is strongly overestimated. However, since the mass of injected CO_2 that dissolves in the formation is proportional to the induced pressure rise. This initial assumption will give realistic storage capacities for CO_2 in the gas-phase and in the fluid phase. However the migration and spatial distribution of the injected CO_2 can not be traced directly. It can only be approximated by gas saturation and pressure changes.

The initial concentration of dissolved CO_2 within the gas-free part of the Hauptsandstein has been assumed to be in equilibrium with CO_2 at production diminished hydraulic pressure gradients in order to avoid CO_2 flow from the CO_2 gas bearing part into the surrounding formation water, which would yield exaggerated storage capacities. CO_2 has not been observed during drilling in the cap rocks and in the underlying carboniferous, thus the numerical model assumes that the respective formation waters contain no dissolved CO_2. For the water bearing part of the storage formation a CO_2 concentration in solution of about half the saturation concentration has been assumed (fig. 16).

For the numerical simulations it is assumed that the disturbance of the temperature field due to the gas production can be neglected and that the final water saturation is constant within the Hauptsandstein reservoir. Uniform distribution of formation water salinity (5.4 molal) is further assumed (fig. 16).

The relative permeability function of Corey (1954, cited in Pruess et al.1999) is used for all lithologies. The capillary pressure function of Leverett (1941, cited in Pruess et al.1999) has been used for the Hauptsandstein and the function of and Milly (1982, cited in Pruess et al.1999) for the other lithologies.

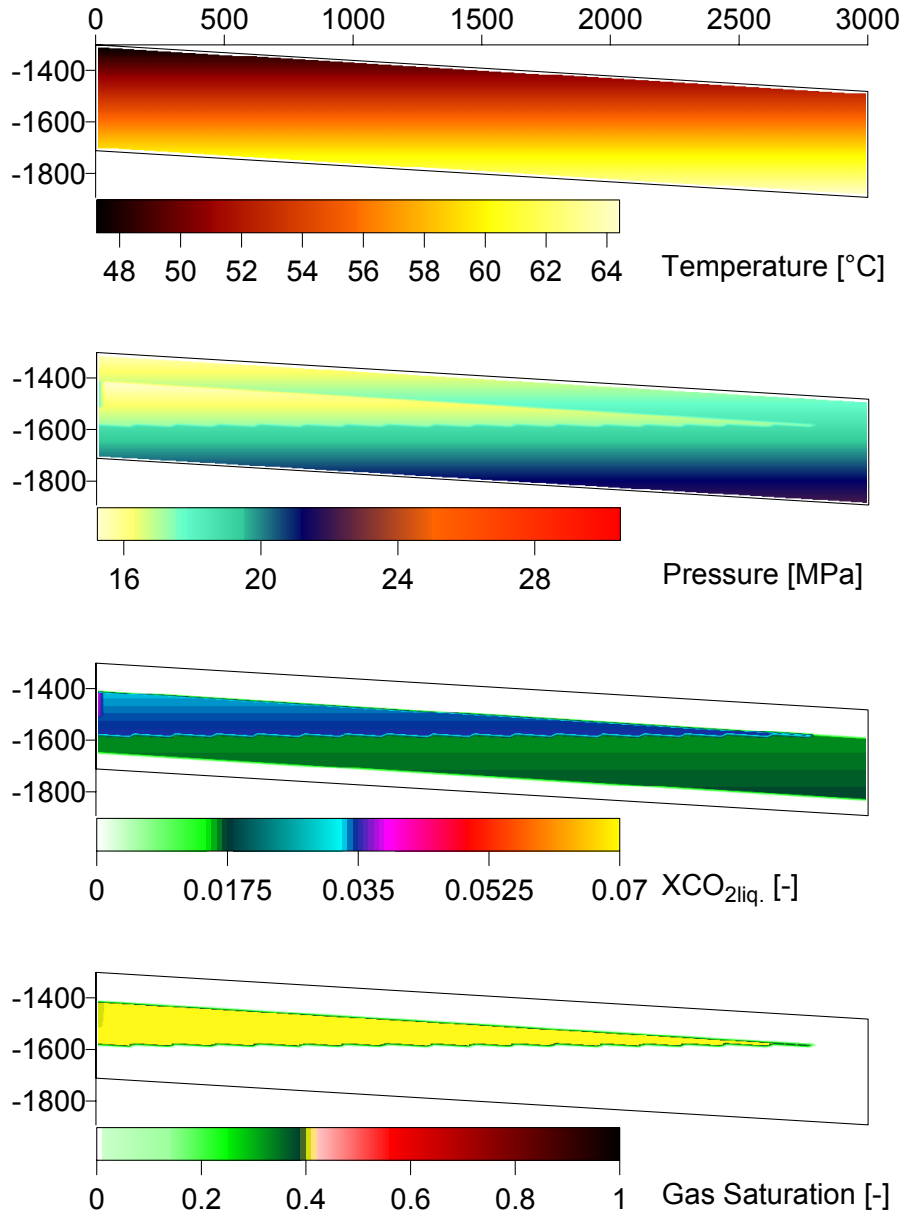

Figure 16. Initial pressure, temperature, gas saturation and XCO_2 distribution in the numerical model, vertical cross sections, dimensions in m.

2.2.3 Results

One of the main issues addressed by the numerical simulations is the calculation of likely injection rates into the low permeable reservoir rocks.

Injection rates have been calculated for three injection scenarios (fig. 17):

1. One central vertical well, 0.2 m effective diameter, perforation length 100 m, within the gas-bearing part of the reservoir, injection pressure 17.5 Mpa (about the initial formation pressure at the top of the gas reservoir).

2. Same layout as above, but injection pressure of 25 MPa (about 1.5 x hydrostatic pressure; compatible with pressure gradients for natural gas storage in porous rocks).
3. One central well with two injection intervals of 100 m length, the upper one at 25 MPa in the gas bearing part of the reservoir, the lower one at 300 MPa, partly reaching down into the water-filled part of the reservoir. Pressure gradients prior to during and after CO_2 injection are shown in (fig. 18).

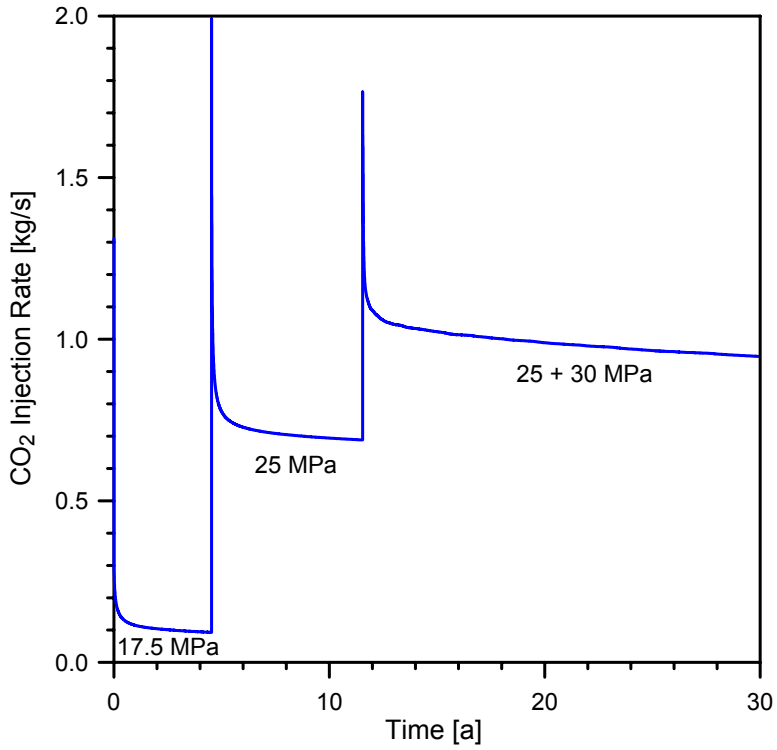

Figure 17. CO_2 injection rates resulting from different injection pressures

The gradual increase of injection rates from step 1 to 3 would represent a phase of pilot projects and technical test. At full load conditions about 1 kg/s or 30 kt/a CO_2 can be injected. In order to inject the CO_2 emitted by the sugar factory during the beet processing season about 10 vertical wells would be required. Thus, horizontal stimulated wells are probably needed for economic CO_2 injection.

With respect to CO_2 injection, expansion, and formation fluid displacement three phases can be distinguished (figure 19, to 25):

1. Injection phase. The injection of CO_2 causes a rapid increase of the fluid pressure in the vicinity of the well. Due to the compression of the surrounding gas, initial injection rates are high, but they decrease soon, after the neighbourhood of the well has been "pumped up". Proportional to the pressure increase, the solubility of gas in the formation water increases, so that the gas saturation in front of the injection area

decreases slightly. A total of 788 kt of CO_2 has been injected over a time period of 29.9 a. The radial extent of the area of high gas saturation is only about 100 m around the injection well (fig. 22), while the over-pressured area with high concentrations of dissolved CO_2 extends to a distance of about 1 km. Radial fluid flow is directed away from the injection well (fig. 19, arrow 1) towards the pressure minimum in about 1 km radial distance and from the deeper marginal parts into the presupposed area of production-induced low pressure reservoir (water drive), (fig. 19, arrow 2). Outwards directed gas migration beneath of the top seal starts at 7.5 a in a distance of 500 m and at 25 a in a distance of 1000 m from the injection well.

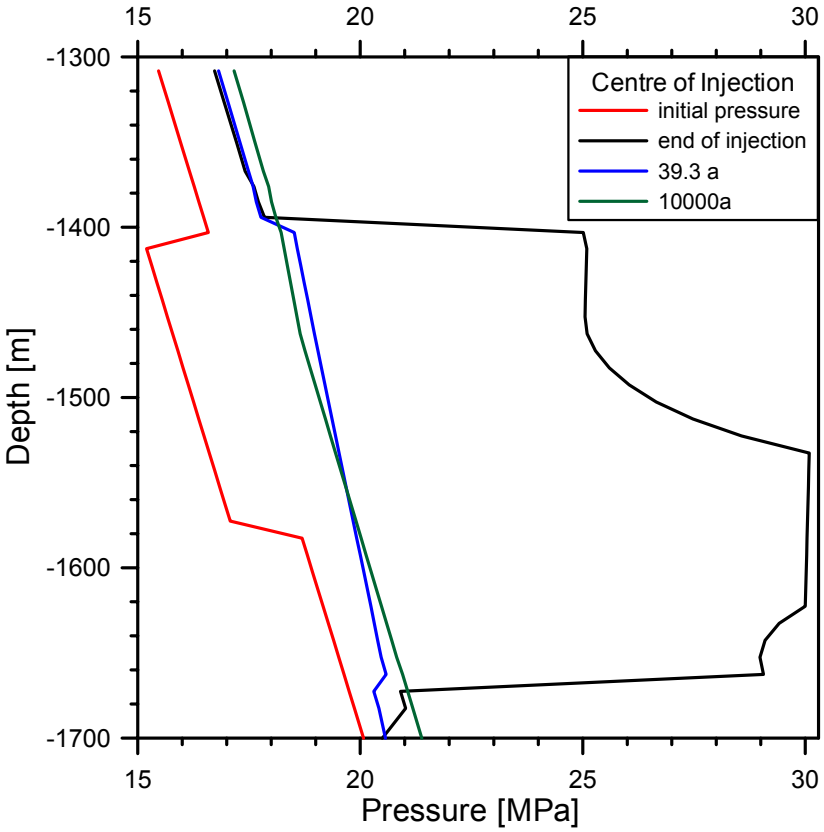

Figure 18. Pressure evolution in the centre of CO_2 injection.

2. Post injection expansion phase. No further water displacement around the lower injection interval occurs in this phase. The gas migrates and expands within the existing two phase area, preferentially along the top of the reservoir. This flow causes a rapid relaxation of the fluid pressures after the termination of CO_2 injection. Maximum lateral gas velocities are reached about 500 m away from the injection well. In the order of 100 a after the injection the induced pressure anomaly is almost balanced (fig. 19).

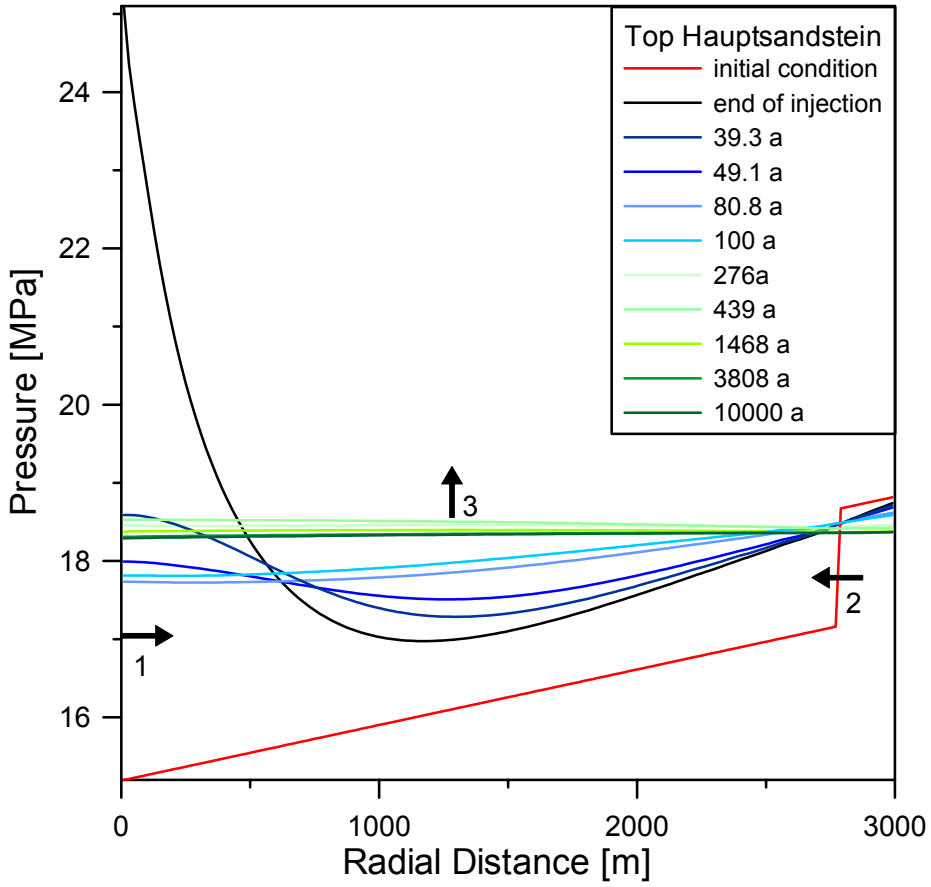

Figure 19. Pressure evolution at the Hauptsandstein top. Arrows indicate main flow directions during and after CO_2 injection.

3. Upwards and lateral gas migration. Buoyant uplift of the gas phase superimposes the lateral gas migration within the Hauptsandstein, causing an accumulation of CO_2 beneath the cap rock of the Wechselfolge (fig. 19, arrow 3). The relative gas permeability increases proportional to the gas saturation at the top of the Hauptsandstein, so that the injected CO_2 spreads out laterally in this layer. The lateral gas flow velocity at the reservoir top slows down to 0.04 m/a within 50 a. Lateral flow velocities of the injected gas reach a maximum at 100 m distance from the well. Further outwards the gas-bearing portion of the reservoir formation pinches out, so that the lateral gas velocities within the wedge of high relative permeability increase again.

   Close to the well maximum vertical gas velocities (peaks in fig. 20, 21) are caused by the rising gas water contact that has been pushed down by the "plug" of injected CO_2. Formation water “flushing” back forces gas to “escape” laterally. The Rotliegend Wechselfolge is penetrated by the rising gas after about 1000 a, creating a corridor for two-phase flow into the lower Zechstein strata. At greater distance the gas phase

invades later into the low permeable rocks of the Rotliegend Wechselfolge and migrates further into the lower Zechstein strata, slowly lowering the pressure in the Hauptsandstein reservoir. Diffusive movement of CO_2 into the formation water below does not increase dissolved concentrations significantly before about 1000 years (fig. 25).

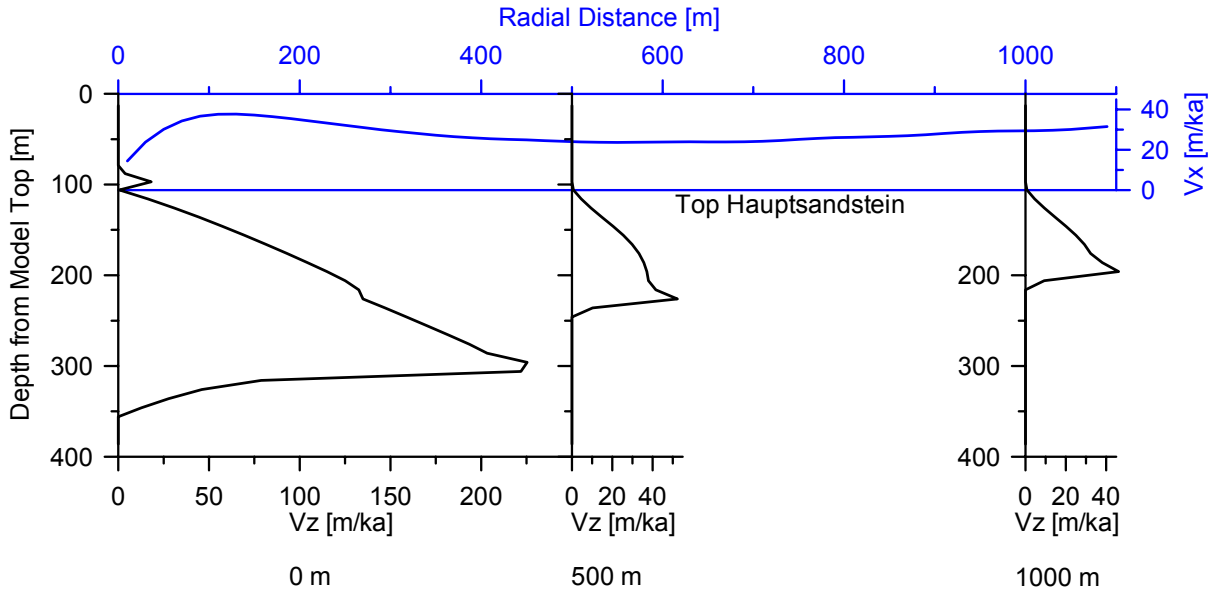

Figure 20. Vertical (Vz) and horizontal (Vx) gas velocities, at 348 years; vertical profiles at 0, 500 and 1000 m distance from the injection well, Horizontal velocities at the top of the Hauptsandstein Reservoir.

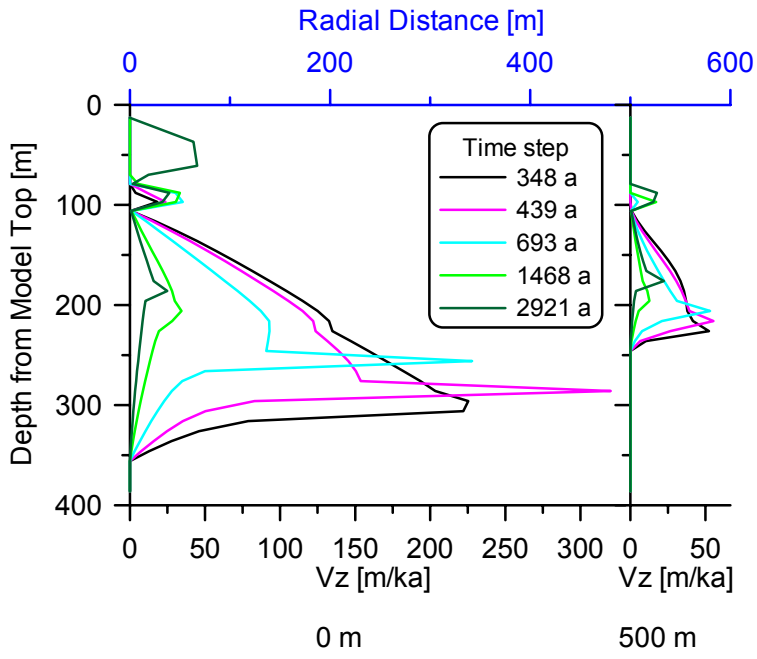

Figure 21. Vertical gas velocities at different time steps; vertical profiles at 0 and 500 m distance from the injection well.

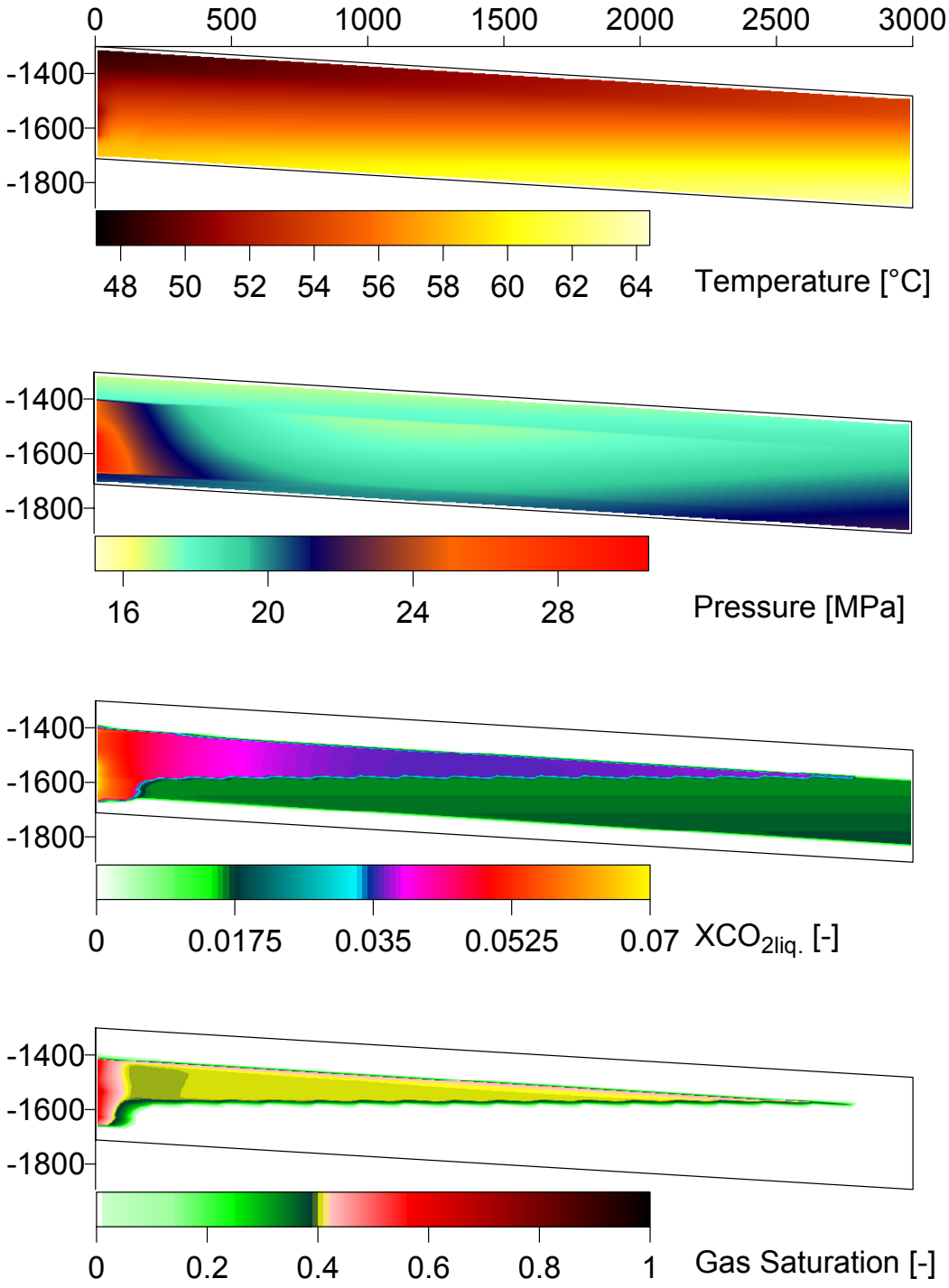

Figure 22. Modelled reservoir conditions after 30 years of CO_2 injection

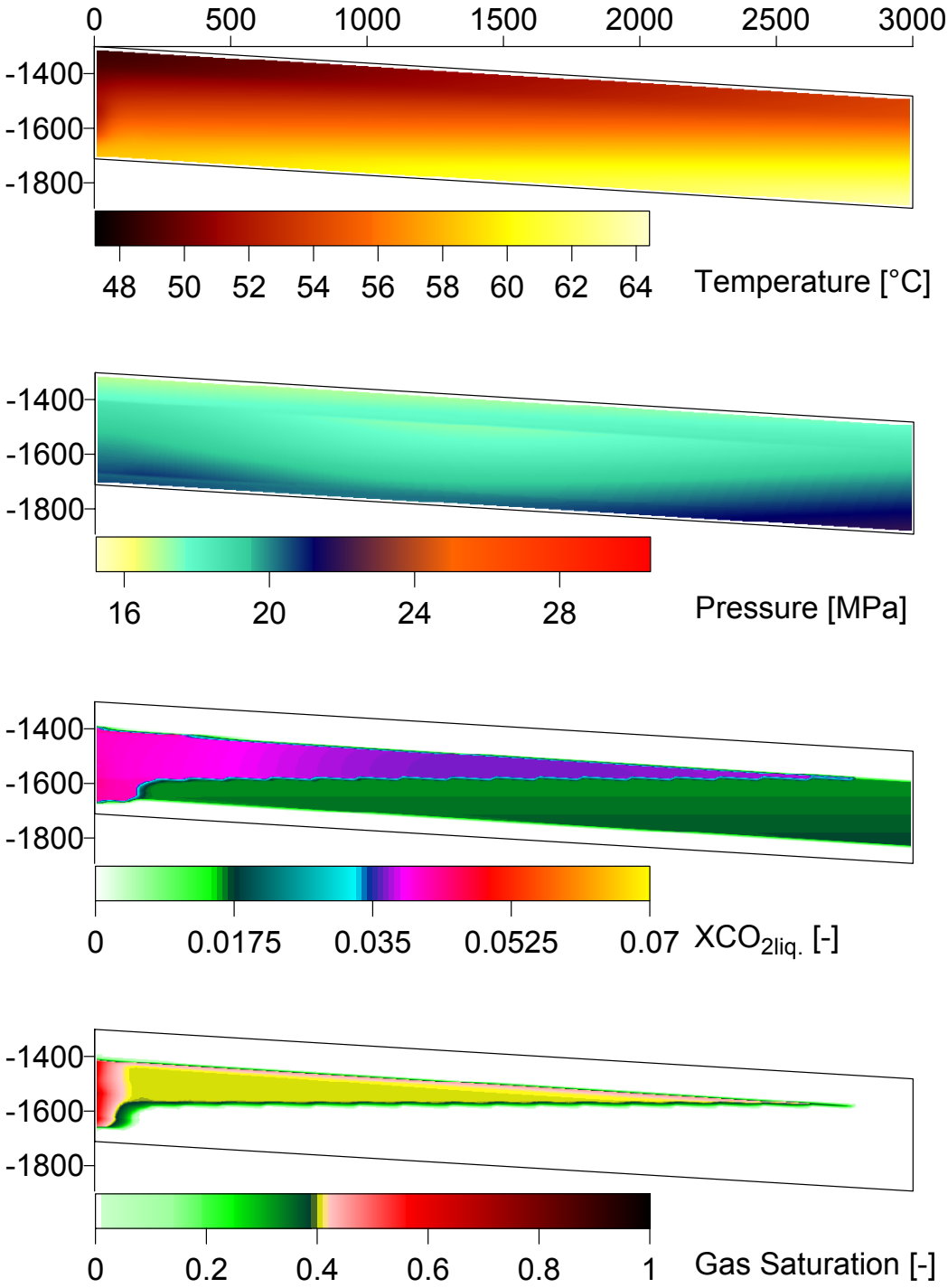

40 a

Figure 23. Modelled reservoir conditions 10 years after the termination of injection

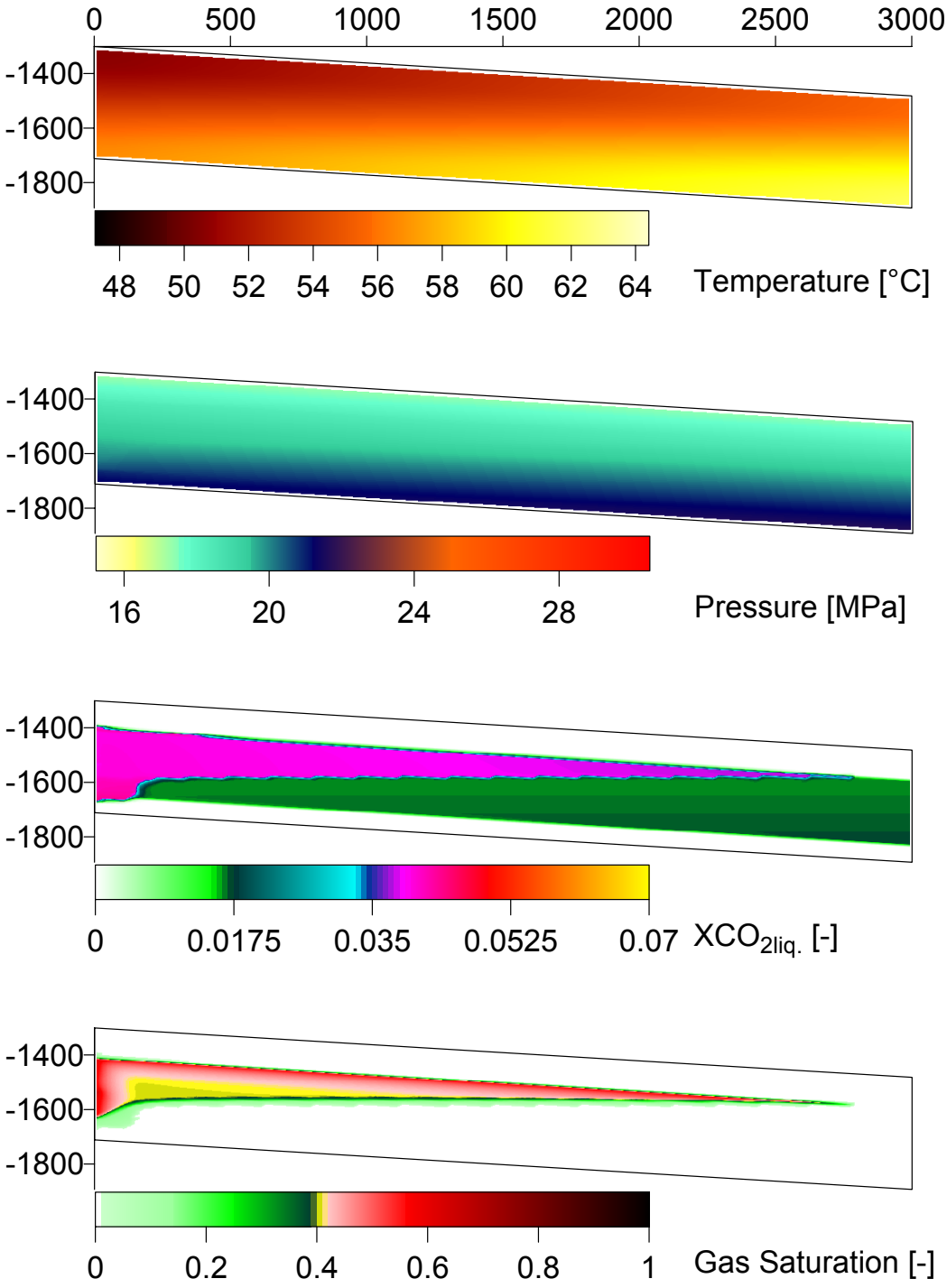

Figure 24. Modelled reservoir conditions 276 years after the start of injection

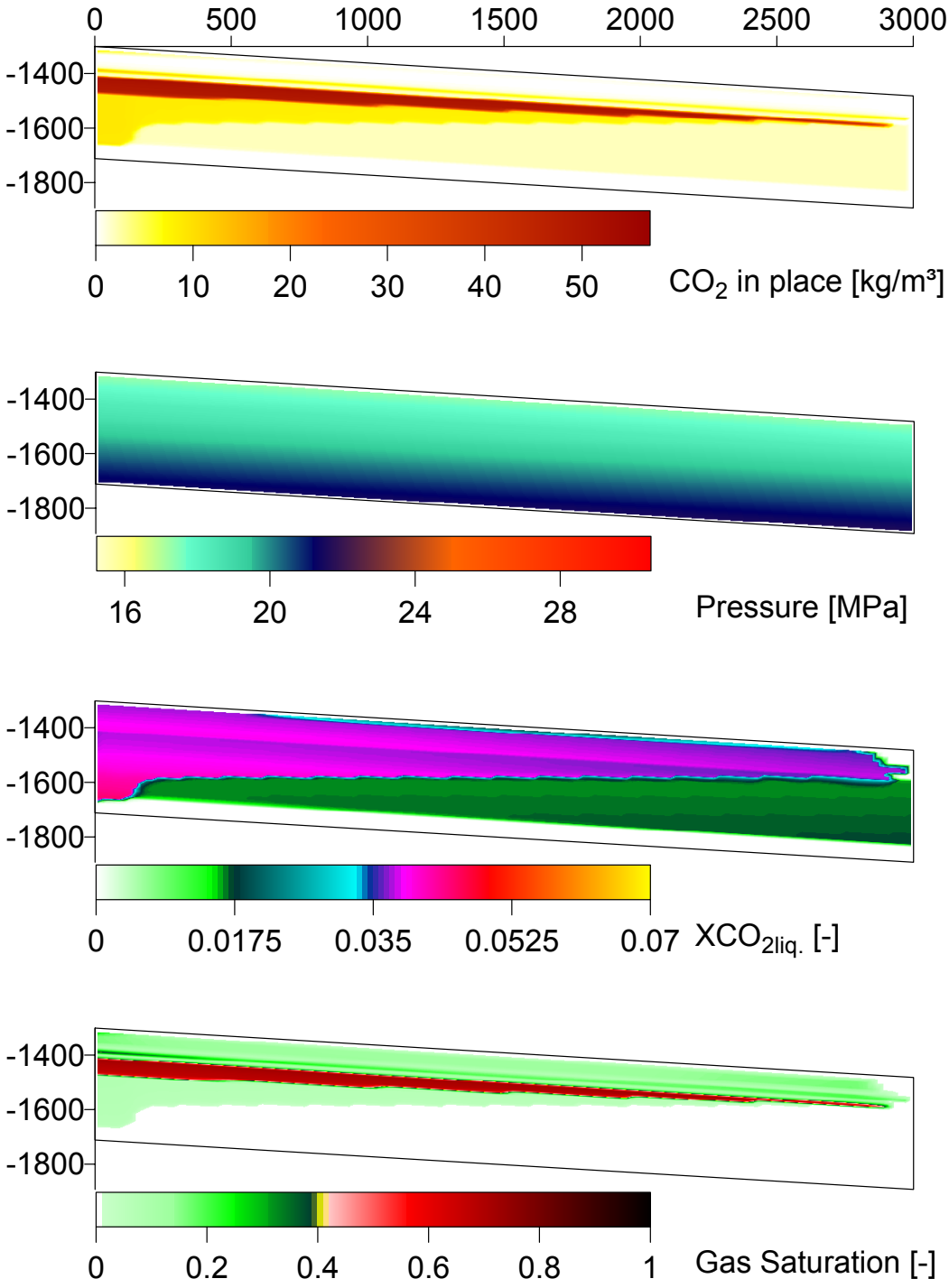

Figure 25. Modelled reservoir conditions 10 000 years after the start of injection

2.2.4 Critique and Limitations

The up-scaling of the measured core porosities and permeabilities appears reasonable since the average injection rate for two injection intervals (0.84 Kg/s) is comparable to the average natural gas production from the three wells in the Alfeld-Elze field (1.09 kg/s). The bulk values are likely a good approximation for the fractured low permeable reservoir sandstone. CO_2 is transported mainly in the gas phase, within the existing two-phase area. Areas of high gas saturation facilitate high gas fluxes due to their good relative permeability.

The fine clastic rocks of the Rotliegend Wechselfolge have been a technical barrier for gas production and CO_2 injection. They are no cap rock that can hold back CO_2 for long times however. This is in accordance with the observation of natural gas in the lower Zechstein carbonate and anhydrite rocks, beneath of the Staßfurt salt which is the actual long term cap rock.

Due to the lack of information, the reservoir model uses constant values for porosity, permeability and initial gas saturation. A reduction of the sweep efficiency due to structural heterogeneity is not considered thus.

The spreading of the injected CO_2 can not be followed directly, because no distinction can be made between the movement of CO_2 injected and the larger amount of CO_2 that had to be present in the two phase area as starting condition. Thus no concentrations of injected CO_2 can be calculated.

Initial pressure distribution determines the fluid flow far from the well. The uniform production induced pressure anomaly of -15 MPa is an extreme situation that exaggerates the effect of water drive from marginal water filled parts of the reservoir. The present pressure distribution is unknown, but probably more levelled, since the simulations indicate a rapid vanishing oft the pressure anomaly around the CO_2 injection well.

Since capillary pressure– and relative permeabilitiy–saturation functions of the cap rocks are not known, the long term CO_2 leakage into the lower Zechstein strata can not be quantified. The model allows no reservoir simulations with justified predictions in time. The simulations should be seen as process simulations only, that help to understand principle steps of gas migration in the given situation within temporal orders of magnitude.

2.2.5 Conclusion

The simulation of two vertically arranged injectors yields low injection rates; about 1/10 of the rate required to inject the CO_2 from the nearby sugar factor. CO_2 is transported mainly as supercritical phase by radial expansion and buoyancy. Gas spreads out along the top of the formation and reaches the margins of trap, though only 16 % of the potential storage capacity (calculated from the gas produced from the Alfeld-Elze field) has been injected.

The vertical injector extending below of the gas–water contact is unfavourable since little water is displaced laterally. Most of the CO_2 rises buoyantly in a communicating tube like area of high gas saturation where gas is pushed down-dip along the Wechselfolge base towards the margins of the structure, so that spill points may be passed. Gas velocities suggest that this marginal gas is mostly gas that has been in the reservoir before the injection started. An array of horizontal wells within the gas bearing part of the reservoir and stimulation of these wells is proposed in order to increase injection rates sufficiently and to use the available storage capacity efficiently. At potential spill points at the margins of gas reservoir additional wells could be used for enhanced gas recovery and to monitor the advent of the injected CO_2.

Rotliegend cap rocks are a technical barrier for CO_2 injection, but no long time barrier. Further petrophysical measurements of core samples and well tests are required in order to quantify leakage rates through the Wechselfolge rocks however. In the end, the integrity of the Zechstein salt has to guarantee long term safety.

2.3 Potential geochemical impact of CO_2-injection

Rotliegend sandstones contain feldspar, clay minerals and carbonates – minerals that can react with CO_2 and formation water. Thermodynamical reaction progress simulations are used to make predictions about the possible effects of geochemical reactions on reservoir rocks and storage capacities.

The mineral composition of the Rotliegend Hauptsandstein samples in the Reservoir Alfeld-Elze has been determined by XRD and by optical microscopy (BEB, unpublished data). Quartz and muscovite/illite are the main mineral phases. Quartz grains are often coated by hematite. Calcite and ankerite are frequent cement phases. Accessory minerals are feldspar, occasionally chlorite and kaolinite/montmorillionite. The high concentrated formation water, (below Zechstein salt in the overburden) is close to halite saturation (BEB, unpublished data).

Besides some assumptions about fluid and mineral compositions, which are required to simulate reactions involving the observed minerals, the basic assumptions for the numerical models are:

- The initial formation water is in equilibrium with CO_2 and N_2 bearing natural gas.
- The model is open for CO_2 (constant pressure), but closed for solids and formation fluid.
- Thermodynamic equilibrium for reaction progress steps is assumed.
- Solid solutions of carbonates are approximated by amounts of the respective end-member minerals.
- The Si concentration of the formation water is assumed to be in equilibrium with Quartz and the Al concentration is in equilibrium with albite respectively.

Three models with different assumptions about protolith phases and mineral stability have been simulated.

1. Full thermodynamic equilibrium, all phases can react (dissolve/precipitate).
2. Illite is meta-stable and does not dissolve
3. Reaction of rocks containing Chlorite but no feldspar.

2.3.1 Model 1, full equilibrium

A typical sandstone composition has been used for the simulations (tab. 5). It is reasonable to assume that the observed plagioclase is Na rich. Though the composition of plagioclase from the Hauptsandstein below Elze is not known, albite is the predominat plagioclase mineral in stratigraphic equivalents of the Hauptsandstein north of Hannover (Hartmann, 1997). Kaolinite is a common alteration product of feldspar weathering and diagenesis. Kaolinisation of albite is also a major alteration reaction of siliciclastic rocks affected by CO_2-rich mineral waters (May et al. 1996). Authigenic formation of feldspar overgrowth on detrital feldspar grains is possible at low diagenetic temperatures and high Na^+/H^+ or K^+/H^+ activity ratios (Pettijohn et al. 1987). Thermodynamic properties of Chalcedony have been used to simulate the precipitation of silica.

Table 5. Sandstone composition used in thermodynamic simulations.

Mineral	Quartz	Illite	Plagioclase	Calcite	Ankerite
Weight Percentage	65	27 $(K_{0.6}Mg_{0.25}Al_{1.8})[\cdots]$	1 $(Ab_{0.95}An_{0.05})$	4 pure	3 $(CaMg_{0.6}Fe_{0.4})\cdots$

The dominant mass transfer in this reaction model is associated with the alteration of illite (fig. 26). Initially kaolinite and chalcedony precipitate until about 20 wt.-% of the wall rock

has been altered. Due to the dissolution of albite, Na concentrations increase and cause the precipitation of some ephemeral halite. The Na^+/H^+ activity ratio also increases until the stability field of albite is reached and albite starts to precipitate, consuming silica and replacing chalcedony as a reaction product of further illite dissolution. Halite dissolves again with progressive rock alteration. Mg released from illite dissolution is consumed in the dolomitisation of calcite reaction. When about 40 wt.-% of the rock has altered, gas liquid and solid phases have attained thermodynamic equilibrium. The amount of authigenic albite exceeds the amount of dissolved albite. The large amount of Na present in the initial formation water is sufficient to facilitate the excess precipitation of albite.

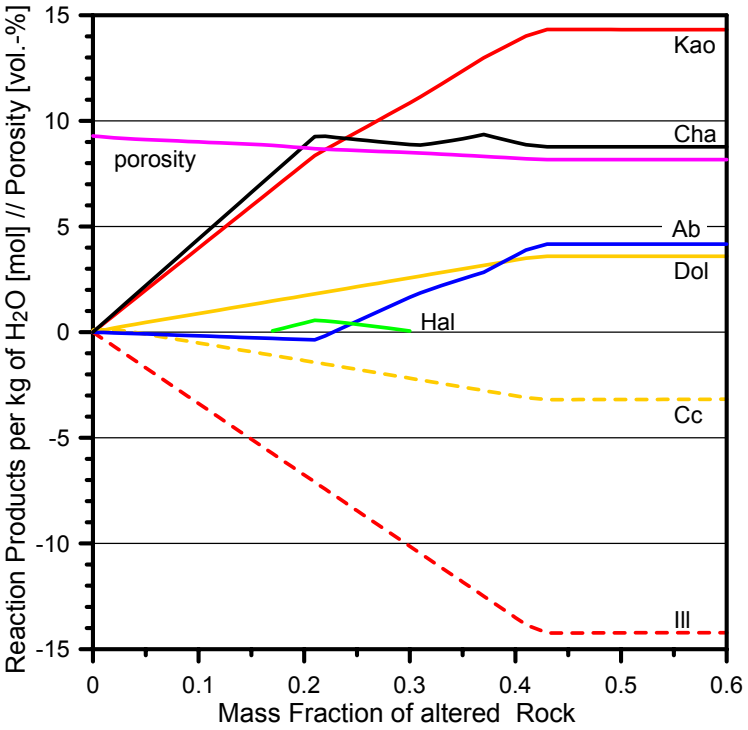

Figure 26. Dissolution of primary phases (negative) and precipitation of solid reaction products (positive) in model 1: Kaolinite (Kao), Chalcedony (Cha), Albite (Ab), Dolomite (Dol), Halite (Ha), Calcite (Cc), Illite (Ill).

Despite a rather large mass transfer from protolith to alterite, the volume change of the solid phases is only small. The rocks porosity would decrease from 9.3 vol.-% initially to 8.2 vol.-% at full water–rock–gas equilibrium.

2.3.2 Model 1a, authigenic K-Feldspar

Since the detrital feldspar in Rotliegend sandstone is albite-rich and authigenic feldspar in natural sediments is usually observed as overgrowth on detrital grains, no K-feldspar formation has been simulated in model 1. However, the simulated solution is strongly supersaturated with respect to K-feldspar. Since XRD analyses can not exclude the presence of minor amounts of K-feldspar, below detection limits, that may serve as nuclei for K-feldspar precipitation, in model 1a the precipitation of both, albite and K-feldspar is

allowed. In this case no full fluid-rock equilibrium is reached (fig. 27). Illite dissolves completely. It is replaced by kaolinite and K-feldspar. Albite precipitates only at a very advanced stage of rock alteration, consuming quartz.

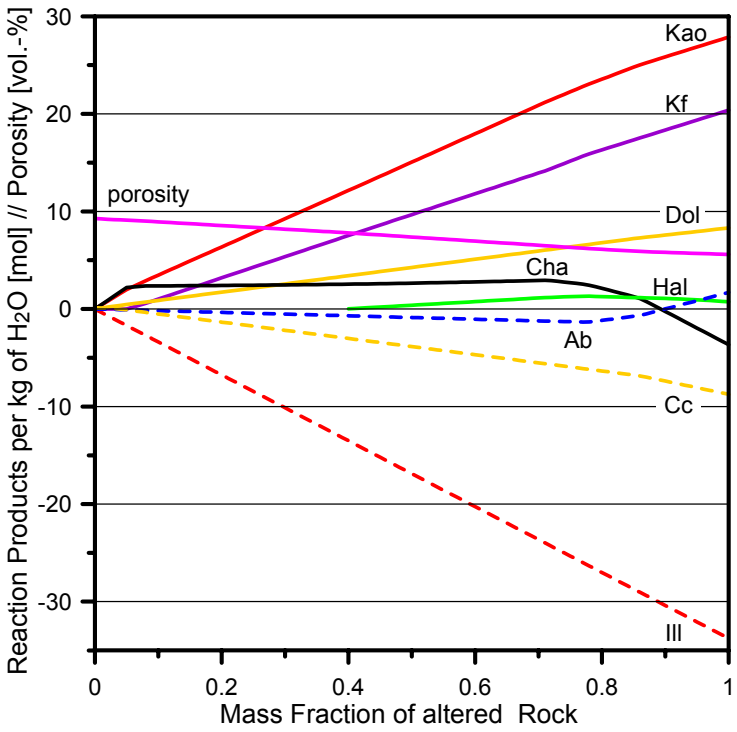

Figure 27. Dissolution of primary phases (negative) and precipitation of solid reaction products (positive) in model 1: Kaolinite (Kao), K-Feldspar (Kf), Chalcedony (Cha), Albite (Ab), Dolomite (Dol), Halite (Ha), Calcite (Cc), Illite (Ill).

2.3.3 Model 2, stable Illite

Though illite is a thermodynamic unstable phase, sandstones and shale from mineral water wells in the Rhineland commonly contain illite. It appears to be involved in the hydrothermal alteration reactions only to a minor degree. Only few samples from strongly altered rocks have illite compositions slightly different from regional protoliths, indicating a possible participation in reactions with the CO_2 rich water (May et al. 1996). Thus a second model is simulated, assuming illite remains stable and Plagioclase is the only reactive mineral. The dominant mass transfer is close to the stoichiometric reaction:

Abite → 0.5 Kaolinite + 2 SiO_2.

The total mass amount of feldspar within a rock volume can be altered without reaching equilibrium with the brine within the pore and fracture space of this volume (fig. 28). Kaolinite and silica are secondary products of plagioclase dissolution. Ca contained in the initial solution and released from feldspar (5-mol-% anorthite component assumed) precipitates as calcite. The maximum porosity reduction for this reaction is negligible (9.3 to 9.25 vol.-%).

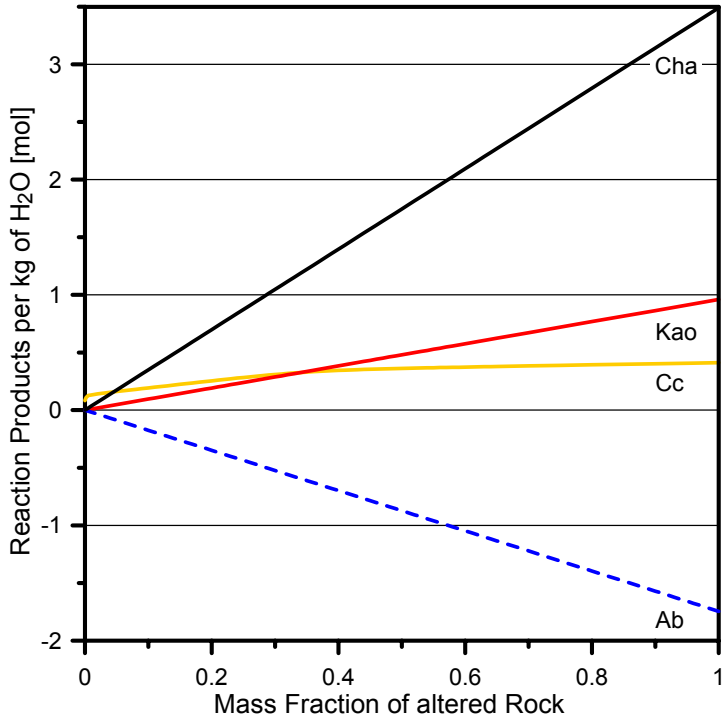

Figure 28. Dissolution of primary phases (negative) and precipitation of solid reaction products (positive) in model 2: Kaolinite (Kao), Chalcedony (Cha), Albite (Ab), Calcite (Cc).

2.3.4 Model 3, Chlorite bearing sandstone

Model 3 simulates the alteration of chlorite bearing sandstone. The chlorite bearing Devonian sandstones affected by CO_2 rich mineral waters in the Rhenish Massif display a range from fresh to completely altered rocks. The dissolution of chlorite is probably a slow kinetically controlled reaction. In the lack of reliable experimental reaction rate data for complex chlorite compositions, the reaction progress approach has been used successfully to simulate slow non-equilibrium alteration reactions of chlorite bearing rocks (May 1998, 1999). This approach indicates the long-term direction of progressive rock alteration.

Sandstone with a typical chlorite content of about 1 wt.-% has been assumed for this simulation. The complete alteration of chlorite to kaolinite, silica and Fe-Mg-carbonate is expected for the modelled open system conditions. At the margins of the CO_2-bearing reservoir part this assumption would not be valid. Thermodynamic data for Fe-free chlorite have been used. Therefor no Fe-carbonate precipitates. The simulated dolomitisation of calcite by Mg released from chlorite is used as a proxy for solid solutions of carbonates that may form. A simplified reaction equation would be:

Chlorite + 5 Calcite → 5 Dolomite + Kaolinite + SiO_2.

The rocks porosity would decrease from 9.3 vol.-% initially to 9.0 vol.-% when all of the chlorite is altered (fig. 29). Though the simulated rock contains only little chlorite, the volume reduction is rather large compared to illite alteration (model 1). The potential for porosity reduction due to CO_2 induced alteration is dependant on variations of the rocks' chlorite content.

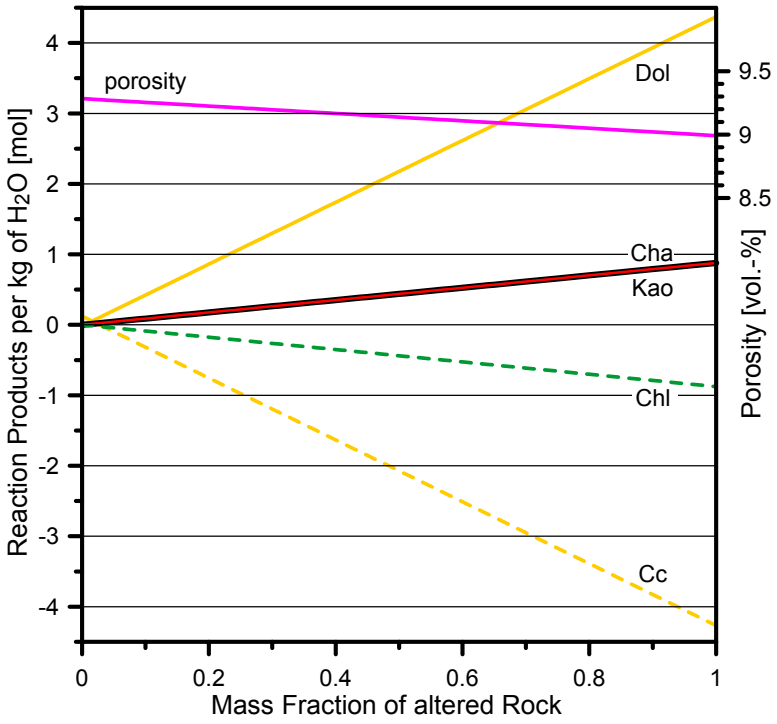

Figure 29. Dissolution of primary phases (negative) and precipitation of solid reaction products (positive) in model 1: Kaolinite (Kao), Chalcedony (Cha), Chlorite (Chl), Dolomite (Dol), Halite (Ha), Calcite (Cc).

2.3.5 Storage Capacity

The contribution of gaseous dissolved and solid carbon species to the total storage capacity is shown in figure 30 as a function of reaction progress for the 4 different reaction scenarios simulated. Porosity reduction may decrease the storage capacity for supercritical CO_2. On the other hand additional CO_2 can be deposited in solid carbonates that result from silicate alteration. The formation water chemistry can also change due to the alteration reactions and thus take up additional CO_2. In model 1, the pH of the formation water changes with progressive rock alteration from acidic (4.1) to neutral (7.3). This causes a shift of the CO_2–HCO_3^- equilibrium, so that the water takes up additional CO_2 to form bicarbonate anions. Little carbonate can precipitate if feldspar is the only reactive mineral. In this case alteration reactions will not cause a significant increase in CO_2 storage capacity. Rocks rich in chlorite can take up a lot of CO_2 and fix it as of Fe-Mg-carbonates. However chlorite contents are generally low and thus even in the case of full alteration, the pore space storage capacity is predominant. If Mg-bearing illite would completely react to

kaolinite and K-feldspar, as provided in model 1a, then a considerable amount of CO_2 could be stored in carbonates, though the total storage capacity would not differ much from model 1 where albite forms. At high degrees of rock alteration the amount of dissolved C-species in the liquid is lower in the initial formation water in equilibrium with the residual natural gas.

If we take alteration conditions in mineral water flow systems of the Rhenish Massif as an indicator that illite will not be reactive and wallrock alteration will remain incomplete, e.g. restricted to fault zones, than geochemical reactions between CO_2, formation water, and the Rotliegend Hauptsandstein probably will not reduce the reservoir porosity very much; nor will solid carbonates be a major sink for the injected CO_2.

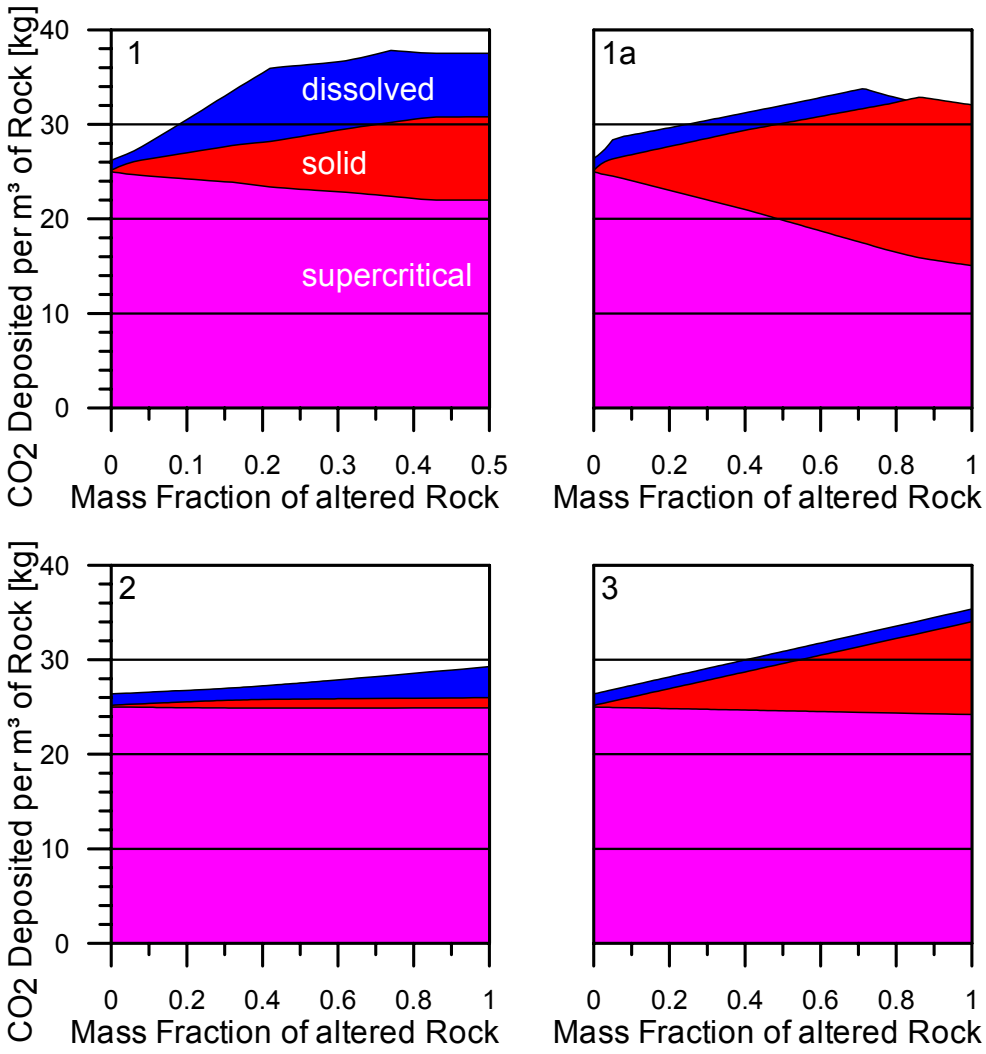

Figure 30. Mass of CO_2 that can be deposited in one cubic meter of reservoir rock at various alteration degrees in supercritical, liquid and solid phases.

2.3.6 Critique and limitations

Though the simulations use some estimates about unknown phase composition and properties, no parameter variations have been performed in order to constrain ranges of uncertainty. Parameter variations would not be able to facilitate a better data interpretation for some basic approximations are made that go beyond mere parameter uncertainty.

- The reservoir may be approximated as a system open for CO_2 during the injection phase. After closing the injection wells, or before in areas of stagnant fluid flow at the margin of the expanding CO_2 front, reaction progress and equilibriums depend on spacial and temporal variable fluid-water-rock ratios. Strong wallrock alteration is likely to occur along gas and fluid conducting faults within the fractured reservoir. Secondary minerals can line fault and fracture surfaces, protecting parts of the reservoir rock from further alteration. Simulated batch mass and volume balances may not be appropriate in this case.

- No information about redox state and couples is available and reactions have been neglected, though Hematite coatings of sand grains might become soluble when reducing exhaust gases are injected. Transport of gas and fluid and reaction velocities are not considered in this model. Though moving reaction fronts may develop creating strong concentration gradients and opportunities for localised mineral precipitation and cementation of the pore space. Dense Fe and Mn oxide sheets are frequent indicators of redox boundaries in sandstones.

- The alteration of silicates by CO_2-bearing water is often slow at low temperatures and natural rocks are often incompletely altered. The reaction progress models do not allow to predict an alteration grade, or mass fraction of rock altered, when the reactions slow down to insignificant rates or come to an end, due to limited amounts of primary phases, or due to the sealing of fresh rocks by alteration products. Advanced degrees of rock alteration may not be achieved within the injection period but only in the long term, or at all. It is not known whether illite is meta-stable or not, and if authigenic feldspar actually precipitates then. Solutions may stay supersaturated when the nucleation or growth of crystals is inhibited.

- Thermodynamic simulations do not allow predictions of the morphotypes of secondary kaolinite. Bulky kaolinite aggregates are known to occur in Rotliegend sandstones (Gaupp et al. 2001). The formation of small amounts of this type of kaolinite may

drastically reduce permeability, especially when it is mobilised in areas of high fluid velocity in the vicinity of injection wells and clogs up pore throats.

Due to these small scale effects that can not be incorporated into the batch reaction progress models, these do not permit predictive simulations. However, they are suitable for process simulations and help to understand processes that might happen. More complex models considering reactive transport and reaction kinetics are also not suitable for predictive modelling (in this and many other cases at least) because they also depend on some basic assumptions, conceptual system boundaries, and additional uncertain parameter. More reliable predictions would require very detailed reservoir fluid characterisation, mineralogical analyses of solid solution phases, mapping of the distributions of porosity, gas saturation and mineral content within the reservoir. Geochemical experiments with reservoir rocks under in-situ-pressure and temperature would be desirable in order to determine appropriate thermodynamics and reaction kinetics for impure and imperfect primary minerals and reaction products. However, reactions involving complex framework and sheet silicates are often rather slow and reliable reaction rates are difficult to obtain by lab experiments. In order to study possible formation damage, caused by the formation and mobilisation of clay minerals, flow-through lab experiments or field test are needed. Geochemical simulations could help to define suitable conditions for such experiments. In the case of the Rotliegend sandstone from Alfeld–Elze experiments could be useful to investigate:

- the stability of illite,
- the likelihood of authigenic feldspar formation,
- the phase composition of secondary carbonate solid solutions,
- the reaction rates of chlorite dissolution,
- and kaolinite morphotypology.

3 References

Bachmann, H. G., J. Mutterlose (1987): Geologie und Erdölgeologie südlich von Hannover. — Führer zu den Exkursionen anlässlich der 139. Hauptversammlung der Deutschen Geologischen Gesellschaft vom 1. – 4. Oktober 1987 in Hannover, p.1–38.

Battistelli, C. Calore, K. Puess (1997): The simulator TOUGH2/EWASG for modelling geothermal reservoirs with brines and non-condensible gas. — Geothermics 26:437–464.

Becker, G., W. Jäger (1973): Gutachten Petrophysik Brg. Loissin 1/70 (Teil I u. II). — VEB Geophysik, Leipzig, 85 p., (unpubl.).

Becker, U., G. Lenz (1992): Zusammenstellung und Auswertung der Testergebnisse ausgewählter Speicher des Mesozoikums. Blatt Rostock/Stralsund. — Geothermie-Engineering GmbH Neubrandenburg; Teilbericht zu Geologische Perspektivitäts-bewertung für die Geothermienutzung in NE-Deutschland Blatt Rostock/Stralsund, Neubrandenburg, p. 205 – 228, (unpubl.).

Beutler, G. (1975): Ergebnisbericht zur Forschungsbohrung E Loissin 1/70 Band 3 Känozoikum – Mesozoikum. — Zentrales Geologisches Institut, Berlin, 127 p., (unpubl.).

Clauser, C., E. Huenges (1995): Thermal conductivity of rocks and minerals. — In: American Geophysical Union (ed.) Rock physics and phase relations. A handbook of physical constants. AGU reference shelf 3, p. 105–126.

Diener, I., J. Wormbs, G. Pasternak, K. Stollberg, M. Tesch, R. Tessin (1992): Geologische Grundlagen zur Geothermienutzung in Nordostdeutschland (Kartenwerk 1:200 000) – Blatt Rostock/Stralsund. — Bundesministerium für Forschung und Technologie, Projektträger (BEO) Biologie, Ökologie, Energie, Forschungszentrum Jülich, Jülich, 228 p., (unpubl.).

Eichler, N. (1987): Geologischer Abschlussbericht zur Suchbohrung Geothermie Stralsund 2–85 (GTSS 2–85). — VEB Geothermie, 27 p. (unpubl.).

Gralla, N. P., F. Nieberding, R. Sobott (1991): Der Wustrow-Sedimentationszyklus des Oberrotliegenden im Bereich einer nordwestdeutschen Erdgaslagerstätte. — Zeitschrift der Deutschen Geologischen Gesellschaft 142:13–21.

Gaupp, R., M. Solms, T. Deutrich (2001): Einfluss der Tonmineralgenese auf das Speicherverhalten von Rotliegendsandsteinen des Nordwestdeutschen Beckens. — DGMK Tagungsbericht 2001-2: 61–68.

Haase, O. (1997): Probleme beim Upscaling hochauflösender geologischer Faziesmodelle zu Gridblockmodellen für die Lagerstättensimulation. — Dissertation Technische Universität Clausthal, 174 p.

Hartmann, B. (1997): Mobilität von Selten-Erd-Elementen und deren Fixierung in Karbonatphasen am Beispiel von Rotliegend-Sandsteinen des Norddeutschen beckens. — Diss. Univ. Mainz, 116 p.

Jordan, H., F. Kockel (1991): Die Leinetal-Struktur und ihr Umfeld. Ein tektonisches Konzept für Südniedersachsen. — Geologisches Jahrbuch, Reihe A 126: 171–196.

Kockel, F. (1984): Geotektonischer Atlas von Nordwestdeutschland 1:100 000, Blatt Hannover, C3922 [Bundesanstalt für Geowissenschaften und Rohstoffe, Hannover].

Lorenz, S., H. Adrian, W. Müller (2001): Modifikationen des TOUGH-Moduls EWASG für einen erweiterten Druck- und Temperaturbereich für CO_2. — 23 p. ISTes report A-615 (unpubl.).

Lüttig, G. (1960): Neue Ergebnisse quartärgeologischer Forschung im Raume Alfeld–Hameln–Elze. — Geologisches Jahrbuch 77: 337–390.

May F., S. Hoernes, H.-J. Neugebauer (1996): Genesis and distribution of mineral waters as a consequence of recent lithospheric dynamics: the Rhenish Massif, Central Europe. — Geologische Rundschau 85: 782-799.

May, F. (1998): Thermodynamic modeling of hydrothermal alteration and geoindicators for CO_2-rich waters. — Zeitschrift der Deutschen Geologischen Gesellschaft 149: 449-464.

May, F. (1999): Contributions to Volcanism, hydrothermal alteration and mineral waters in Northland, New Zealand. — Shaker Verlag, Aachen, 73 p.

Mayer, P., Krauß, M., Wirth, H. (1998): Abschlußbericht zum Projekt SASO II Erfassung des präquartären Strukturbaus der östlichen Boddengewässer Vorpommerns und angrenzenden Ostsee anhand geologischer und reflexionsseismischer Daten. — Ernst-Moritz-Arndt-Universität Greifswald, 92 p. + maps and extensions.

Pettijohn, F. J., P. E. Potter, R. Siever (1987): Sand and Sandstone. — 2nd edition, Springer, 553p.

Pruess, K., C. Oldenburg, G. Moridis (1999): TOUGH2 User's guide, version 2.0. — Lawrence Berkeley National Laboratory Publication 43134, 197 p.

Reinicke, R. (1968): Ergebnisbericht der Bohrung E-Wusterhusen 1/67. — VEB Erdöl und Erdgas Grimmen, Grimmen, 108 p.(unpubl.).

Reinicke, R. (1970): Ergebnisbericht der Bohrung E-Greifswalder Bodden 1/69. — VEB Erdöl und Erdgas Grimmen, Grimmen, 268 p.(unpubl.).

Rudolph, H., G. Gärtitz, U. Lehmkuhl, I. Rudolph, H. Weyrich, K.-D. Zimmermann, H. Zwahr, D. Häußer, S. Müller, H.-D. Peters (1972): Bericht über lithologisch-petrophysikalische Untersuchungen zum F/E-Thema "Gasabgabefähigkeit der

Schluffsteine im Rotliegenden des Strukturbereiches Salzwedel-Peckensen". — Forschungsinstitut für die Erkundung von Erdöl und Erdgas, Gommern, 844 p.

Sauer, A. (1976) Geologisch-technisch-ökonomischer Abschlußbericht der Suchbohrung E-Lubmin 3-75. — VEB Erdöl und Erdgas Grimmen, Grimmen, 66 p.(unpubl.).

Sauer, A. (1979) Geologisch-technisch-ökonomischer Abschlußbericht der Bohrung E Wusterhusen 3-79. — VEB Erdöl und Erdgas Grimmen, Grimmen, 37 p.(unpubl.).

Sedlacek, R., G. Stancu-Kristoff (1993): Disposal von Lagerstättenwässern in der Bohrung Hildesheimer Wald Z1 (Rotliegend). — Gutachten Niedersächsisches Landesamt für Bodenforschung, Hannover, 5 p., (unpubl.).

Schlömer, S., B. Krooss (1997): Experimental characterisation of the hydrocarbon sealin efficiency of cap rocks. — Marine and Petroleum Geology 14,5: 565–580.

Schröder, L., E. Plein, G. H. Bachmann, R. E. Gast, U. Gebhardt, R. Graf, H.-J. Helmuth, M. Pasternak, H. Porth, S. Süssmuth (1995): Stratigraphische Neugliederung des Rotliegenden im Norddeutschen Becken. — Geologisches Jahrbuch A148: 3–21.

R. Schulz, H.-G. Röhling (2000): Geothermische Resourcen in Nordwestdeutschland. — Zeitschrift für angewandte Geologie 46,3: 122–129.

Steinhoff, I. (1995): Ca2-Faziesstudie in den Erlaubnisfeldern Alfeld und Hildesheimer Wald. — Endbericht, Niedersächsisches Landesamt für Bodenforachung, Hannover, 29 p., (unpubl.).

Winter, I., V. Meyn (1997): Physical investigations of the electrical and capillary properties of reservoir rocks at simulated reservoir conditions. — DGMK-Forschungsbericht 494-2, Hamburg, 36 p.

Wirtschaftliche Vereinigung Zucker e.V. (2001): Zucker aus Rüben — Bonn 34 S.

Ziegenhardt, W., W. Brandt, R. Jagsch (1997): Strukturelle Charakteristik eines Kluftspeichers im sedimentären Rotliegenden. — Zeitschrift für angewandte Geologie 23: 618–625.

4 Acknowledgements

Work documented in this report has been financially supported by the European Community under contract number ENK6-CT-1999-00010 „GESTCO“.
Exxon Mobile Production Germany (formerly BEB) kindly provided information on the gas field Alfeld-Elze.

Bundesanstalt für Geowissenschaften und Rohstoffe

Im Auftrage

……

Dr. Franz May

- wiss. Angestellter -

……

Dr. Peter Gerling

- Geologiedirektor -

……

Dr. Paul Krull

- Geologiedirektor -